

# Waveform distortion for temperature compensation and synchronization in circadian rhythms:

## An approach based on the renormalization group method

Shingo Gibo <sup>\*1</sup>, Teiji Kunihiro<sup>2</sup>, Tetsuo Hatsuda<sup>1</sup>, and Gen Kurosawa <sup>†1</sup>

<sup>1</sup>Interdisciplinary Theoretical and Mathematical Sciences Program (iTHEMS), RIKEN

<sup>2</sup>Yukawa Institute for Theoretical Physics (YITP), Kyoto University

### Abstract

Numerous biological processes accelerate as temperatures increase, but the period of circadian rhythms remains constant, known as temperature compensation, while synchronizing with the 24h light-dark cycle. We theoretically explore the possible relevance of waveform distortions in circadian gene-protein dynamics to the temperature compensation and synchronization. Our analysis of the Goodwin model provides a coherent explanation of most of temperature compensation hypotheses. Using the renormalization group method, we analytically demonstrate that the decreasing phase of circadian protein oscillations should lengthen with increasing temperature, leading to waveform distortions to maintain a stable period. This waveform-period correlation also occurs in other oscillators like Lotka-Volterra and van der Pol models. A reanalysis of known data nicely confirms our findings on waveform distortion and its impact on synchronization range. Thus we conclude that circadian rhythm waveforms are fundamental to both temperature compensation and synchronization.

**Keywords:** waveform distortion, renormalization group method, circadian rhythms, temperature compensation, synchronization

### Author Summary

Our daily rhythms are underlain by gene regulatory and biochemical networks, called circadian clocks. Although most biochemical reactions accelerate as temperature increases, the period of

---

\*shingo.gibo@riken.jp

†g.kurosawa@riken.jp

circadian rhythms is almost constant even with increasing temperature. This phenomenon is called temperature compensation, and the mechanism is still unclear. By applying a method of theoretical physics, the renormalization group method to a biological problem for the first time, we revealed that the waveform of gene dynamics should be more distorted from sinusoidal wave at higher temperature when the circadian period is stable to changes in temperature. This prediction as for the importance of waveform in temperature compensation is verified by analyzing published experimental data. Notably, the correlation between period and waveform distortion holds for other oscillator models, indicating the waveform distortion is important for determining the period in various types of oscillatory systems. Another unsolved problem of circadian clocks is to synchronize with environmental light-dark cycles. By theoretically analyzing a circadian clock model, we found that the frequency range for synchronization becomes narrower when the waveform is distorted.

## 1 Introduction

Humans exhibit sleep-wake cycles with an approximate 24h period, and these cycles persist under constant environmental conditions, a phenomenon termed the circadian rhythm. This temporal regulation exists in both humans and various organisms such as molds, plants, and insects [1, 2, 3]. Recent advances in genetic research through insects, molds, mammals, and plants have unveiled that genes and proteins are involved as integral components in the primary mechanism governing autonomous circadian rhythms [1, 4, 5, 6].

Understanding circadian rhythms holds promise for deciphering a multitude of sleep patterns, including sleep disorders such as advanced sleep phase syndrome (characterized by early awakening around 4:00 am), delayed sleep phase syndrome (marked by late awakening), non-24h sleep-wake disorder, and narcolepsy [7]. Notably, advanced and delayed sleep phase syndromes are believed to be linked to the circadian rhythm period [8, 9, 10, 11, 12, 13]. Ongoing studies explore possible correlations between genetic characteristics revealed by large-scale genetic analysis and various sleep patterns [14, 15, 16]. However, the nature of the system is so intricate that it remains a challenge to link sleep patterns to specific genes. In such a situation, it would be meaningful to have recourse to mathematical models and obtain possible hints for the linkage and hopefully suggestions for studies of genetic dynamics.

One unresolved fundamental issue in circadian rhythm research is temperature compensation

[17, 18, 19, 20, 21, 22, 23, 24, 25] , in which the period keeps constant despite temperature-induced changes in reaction rates. Despite the extensive experimental and theoretical research on temperature compensation, the mechanism has remained elusive. Hypotheses have been proposed to explain temperature compensation, including the balance hypothesis, critical-reaction hypothesis, temperature-amplitude coupling hypothesis, and waveform hypothesis. The balance hypothesis proposes that the stability of the circadian period with temperature arises from a balance between period-lengthening and period-shortening reactions [17, 18, 26]. The critical-reaction hypothesis assumes that there should be critical reactions that determine the circadian period. If these reaction rates are stable against temperature variations, then the circadian period will similarly remain stable [27, 28, 29]. The temperature-amplitude coupling hypothesis suggests that temperature-sensitive amplitudes in gene activity rhythms should generate a stable period by generating larger amplitudes at higher temperatures [22, 30]. Lastly, the waveform hypothesis proposes that temperature-sensitive waveforms in gene activity rhythms should be correlated with a stable period in a manner that their higher harmonic components become larger and the distortion of the waveform increases at higher temperatures [31].

Another unresolved issue in circadian rhythm research is synchronization with 24h environmental light-dark cycles. Previous theoretical and experimental studies on synchronization revealed that if the internal period of the oscillation closely matches the external period, then it is more likely to synchronize with the forced period [32, 33, 34, 35]. Additionally, experimental studies on several species uncovered genes and proteins in circadian systems affected by a light pulse [36, 37]. In reality, the circadian rhythm must adjust to the 24h light-dark cycle while maintaining a temperature-compensated circadian period. Therefore, multiple questions arise. (i) Given the significant temperature variations between seasons, how do organisms synchronize their circadian rhythms with the 24h light-dark cycle across various temperatures [20, 34, 38]? (ii) if the gene activity rhythm of the circadian rhythms becomes more distorted as temperatures increase to achieve temperature compensation, how does the ease of synchronization change with temperature variations? Theoretical analyses incorporating the findings of light pulse experiments might provide further insights into these questions.

In the present paper, we investigate possible roles of the waveform distortion in temperature compensation based on analytical and numerical analyses of the Goodwin model for circadian rhythms and clarify how the waveform in gene activity rhythms tends to be more distorted

at higher temperatures (e.g., steeper rise, longer tail) for temperature compensation. To this end, we employ the renormalization group (RG) method, a powerful tool for analyzing various non-linear systems described by ordinary and partial differential equations, to derive global solutions that are valid in a global time domain [39, 40, 41, 42, 43, 44, 45, 46, 47, 48, 49, 50, 51, 52, 53, 54].

Combining an index for waveform distortion, namely non-sinusoidal power ( $NS$ ) introduced by two of the present authors (KG) [31], with the result of the RG method, we can obtain both a unified picture of the above mentioned theoretical hypotheses (balance hypothesis, critical-reaction hypothesis, temperature-amplitude coupling hypothesis, and waveform hypothesis) and quantify previous experimental data on *Drosophila* [55]. Our analyses demonstrate that the fundamental role of the waveform distortions in temperature compensation from both theoretical and experimental perspectives in accordance with the previous findings [31]. Moreover, we reveal for the first time the mechanism by which the synchronization of circadian rhythms changes with temperature if the waveform in gene activity rhythms is more distorted at higher temperatures. We theoretically prove that the frequency range of the external force that synchronizes circadian rhythms becomes narrower if the waveform of gene activity rhythms is more distorted. This indicates that it is more difficult to synchronize with light-dark cycles at higher temperatures. The present result of synchronization is consistent with the previous experimental and numerical studies demonstrating that the magnitude of the phase shift caused by light pulses was smaller at higher temperature [31, 56, 57].

## Results

### 2 Waveform distortion in circadian rhythms

#### 2.1 Index for waveform distortion

Let the time dependence of a certain variable in the circadian rhythm system be expressed in a Fourier series as  $x(t) = \sum_{j=-\infty}^{\infty} a_j \exp(i(\frac{2\pi}{\tau})jt)$ , with  $a_j$  being the Fourier coefficients of the oscillatory time series. Then, we introduce an index for describing the distortion of  $x(t)$  from a sinusoidal shape as

$$NS = \left[ \frac{\sum_{j=1}^{\infty} |a_j|^2 j^m}{\sum_{j=1}^{\infty} |a_j|^2 j^q} \right]^{\frac{1}{2}} \quad (m > q \geq 0), \quad (1)$$

where  $m$  and  $q$  are integers. Termed the "non-sinusoidal power ( $NS$ )", this index is designed to emphasize higher harmonics ( $m > q$ ) as discussed in a previous paper [31]. For instance, we have  $NS = 1$  when the time series has a sinusoidal waveform in which only the coefficients for the fundamental component are non-zero ( $a_{\pm 1} \neq 0$ ). Conversely, for non-sinusoidal time series, the coefficients for higher harmonics are non-vanishing, resulting in  $NS > 1$ . The previous theoretical work demonstrated that a more distorted waveform (larger  $NS$ ) at higher temperature is necessary for temperature compensation in the four-variable negative-feedback model [31]. However, it is unclear whether the relevance of waveforms to temperature compensation found in previous research has general validity not restricted to some specific model.

To explore the possible relevance of the waveform characteristics to temperature compensation and synchronization, we consider the simplest model for circadian rhythms, known as the Goodwin model (Fig. 1A) [58]. This model incorporates negative-feedback regulation of gene expression, a mechanism established as essential for transcriptional-translational oscillations. The three-component Goodwin model reads:

$$\frac{dx_1}{dt} = f(x_3) - k_1x_1, \quad (2)$$

$$\frac{dx_2}{dt} = p_1x_1 - k_2x_2, \quad (3)$$

$$\frac{dx_3}{dt} = p_2x_2 - k_3x_3, \quad (4)$$

where  $x_1(t)$  represents mRNA abundance, and  $x_2(t)$  and  $x_3(t)$  denote protein abundance. The function  $f(x_3)$  in the model signifies transcriptional regulation, and the parameters  $p_1$  and  $p_2$  denote protein synthesis and phosphorylation rates, respectively, and  $k_i$  ( $i = 1, 2, 3$ ) represent degradation rates (Fig. 1A). By applying signal processing methods, Forger derived the period of this model as follows [59]:

$$\tau = \frac{2\pi}{\sqrt{k_1k_2 + k_2k_3 + k_3k_1}} \left[ \frac{\sum_{j=1}^{\infty} |a_j|^2 j^4}{\sum_{j=1}^{\infty} |a_j|^2 j^2} \right]^{\frac{1}{2}}. \quad (5)$$

Subsequently, two of the present authors indicated that this formula implies that temperature compensation of the period in this model occurs only when the waveform ( $NS$ ) is distorted as temperature increases [31]. Suppose that all reactions become faster as temperature increases in the model. Then, one can numerically demonstrate that the waveform tends to be more distorted (larger  $NS$ ) at higher temperatures for temperature compensation (Fig. 1B, magenta

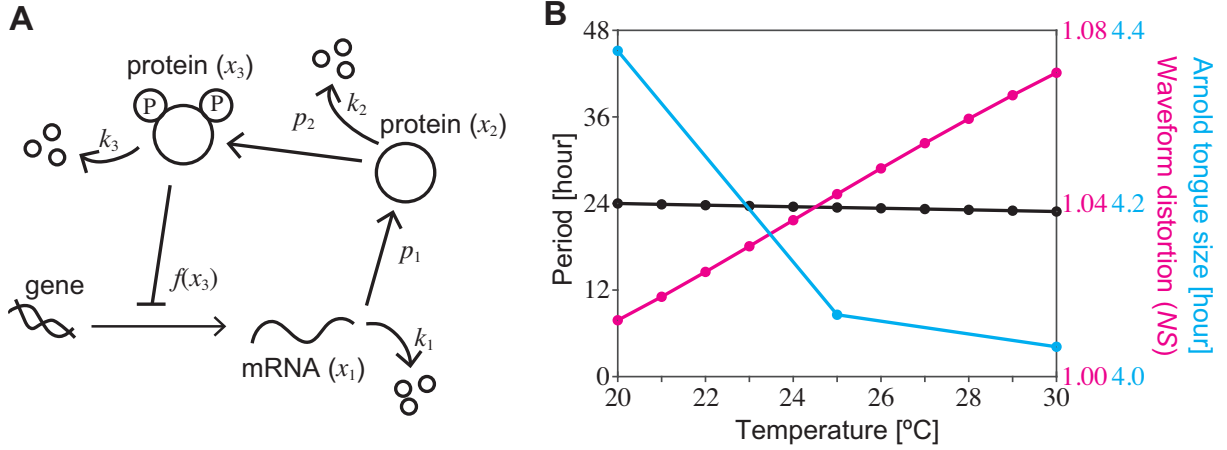


Figure 1: (A) The circadian clock model and (B) the relevance of waveform characteristics to temperature compensation (*magenta*) and synchronization (*cyan*). The transcriptional-translational function is defined as  $f(x_3) = r/(1 + (x_3/K)^n)$ , with the values of  $K$  and  $n$  set to be 0.0184 and 11, respectively. Assuming that the parameters  $k_1$ ,  $k_2$ ,  $k_3$ ,  $p_1$ ,  $p_2$ , and  $r$  increase with increasing temperature, we model the reactions rates using the Arrhenius law  $b_i = A_i \exp(-E_i/RT)$ , where  $b_i$ ,  $E_i$ ,  $A_i$ ,  $R$ , and  $T$  are the rate constants, activation energies, frequency factors, gas constant ( $R = 8.314$ ), and absolute temperature, respectively. The values of  $E_i$  and  $A_i$  are detailed in Supplementary Table 1. The synchronization region depends on the period of light-dark cycles and light intensity, known as the Arnold tongue [35]. The size the Arnold tongue is defined by the difference between the lower limit of synchronization,  $2\pi/\Omega_{\text{large}}$ , and the upper limit of synchronization,  $2\pi/\Omega_{\text{small}}$ .

When the period is constant in a different temperature, the waveform distortion ( $NS$ ) becomes larger, and the synchronization range (size of the Arnold tongue) becomes narrower with increasing temperature as shown in (B) in the case of the light intensity,  $I = 0.001$ .

line). We call this mechanism the waveform hypothesis for temperature compensation.

## 2.2 Theories of temperature compensation

The waveform hypothesis and the other three hypotheses for temperature compensation (balance hypothesis I, critical-reaction hypothesis II, and amplitude hypothesis III) are not mutually exclusive, which can be understood in a unified way through Eq. (5):

- I. The balance hypothesis, previously explored theoretically by Ruoff [18], suggests that the temperature compensation of the period is caused by a balance between the effects of reactions that shorten the period and those that lengthen the period. Equation (5) illustrates that the balance between the effect of shortening the period and that of lengthening the period can be caused by changing the distortion of the waveform.
- II. Equation (5) demonstrates that even if some of the governing reactions in circadian rhythms are temperature-insensitive [27, 29] as discussed in the critical-reaction hypothesis. Still,

the temperature compensation requires waveform distortion at high temperatures if reactions other than some of the governing reactions accelerate at higher temperatures.

III. Our numerical analysis of the circadian model (Fig. 1B) show that when temperature compensation occurs, the waveform is more distorted at higher temperatures, and the amplitude of the oscillation is larger. This tendency for the amplitude to increase at high temperatures is consistent with the amplitude hypothesis. According to Eq. (5), a greater distortion of the waveform at higher temperatures is necessary, but not sufficient, for temperature compensation.

### 2.3 Synchronization in circadian rhythms

If the waveform is more distorted at higher temperatures for temperature compensation, then it would be intriguing to explore whether the temperature-dependent waveform also affects the synchronization of circadian rhythms with environmental light-dark cycles at various temperatures. Theoretical and experimental studies of synchronization and circadian rhythms illustrated that the oscillation is more likely to synchronize with forcing cycles if the internal period is sufficiently close to the period of the forcing cycles [32, 33, 34, 35]. In mammals and *Neurospora*, a light pulse is known to increase *Per1* and *frq* mRNA expression [36, 37]. To incorporate gene activation during the light phase, we employ a model in which Eq. (2) for the change in mRNA expression is modified to

$$\frac{dx_1}{dt} = f(x_3) - k_1 x_1 + I \cos(\Omega t), \quad (6)$$

where  $I$  represents the light intensity and  $\Omega$  is the angular frequency of the light-dark cycles.

### 2.4 Main results

In Sections 3 and 4, we provide detailed discussions on how the waveform in gene activity rhythms should be distorted at higher temperatures using the RG method, as well as the synchronization in circadian rhythms. The main results are pictorially summarized in Fig. 1B. The magenta line indicates that the waveform of the gene activity rhythms should be more distorted at higher temperatures for temperature compensation, whereas the cyan line indicates that synchronization with the light-dark cycles should become more difficult at higher temperatures because of the larger waveform distortion.

### 3 Waveform distortion and temperature compensation

#### 3.1 Numerical simulation of the waveform-period correlation

Equation (5) and numerical simulations indicate that  $NS$  tends to be larger when the period is relatively stable even with increased parameter values (see Fig. 1B). To quantitatively reveal the correlation between waveform and period, we conduct numerical simulations using a circadian clock model. In the analysis of the circadian clock model, the transcription function  $f(x_3) = r/x_3^n$  was considered for simplicity. We first search for parameter sets in which oscillations occur. We define those parameter sets as the reference parameter sets. Because many biochemical parameters have not yet been measured, we prepared 100 random reference parameter sets for the oscillations.  $k_1, k_2, k_3, p_1, p_2,$  and  $r$  were assigned uniformly distributed random values ranging from 0 to 10, and  $n$  was assigned a uniformly distributed random integer ranging from 9 to 15. The period obtained with each reference parameter set was denoted as  $\tau_1$ . Next, reaction rates often follow the Arrhenius equation, which states that a 10°C rise in temperature increases the reaction rate by a factor of 2-3. To incorporate the effect of high temperature, instead of using the Arrhenius equation, each parameter in the model's reference parameter set was randomly multiplied by a factor of 1.1-1.9, and the period and waveform were examined when the oscillation behavior persists. The period obtained by increasing the parameters from each reference parameter set was denoted as  $\tau_2$ , and the ratio,  $\tau_2/\tau_1$ , was called the relative period.

To quantitatively analyze the correlation between period and waveform when temperature compensation occurs, we consider the case of the relative period  $\geq 0.85$  because it has been experimentally confirmed that the circadian rhythm frequency at high temperature divided by that at low temperature of the wild-type ranges between 0.85 and 1.15 when the temperature is increased by 10°C and temperature compensation occurs [19]. In the present numerical analysis, the period is relatively stable (relative period  $\geq 0.85$ ) in 34 of the 4900 parameter sets, in qualitative agreement with previous theoretical analyses that the period often shortens with increasing reaction rates [18, 26]. Because the range of parameter variation is 1.1-1.9 and the average value is 1.5, the reaction rate is accelerated by a factor of 1.5 on average, and the average relative period is approximately  $1/1.5 \approx 0.67$ . Figure 2 indicates that when temperature compensation occurs, there is a clear correlation between the period and waveform.



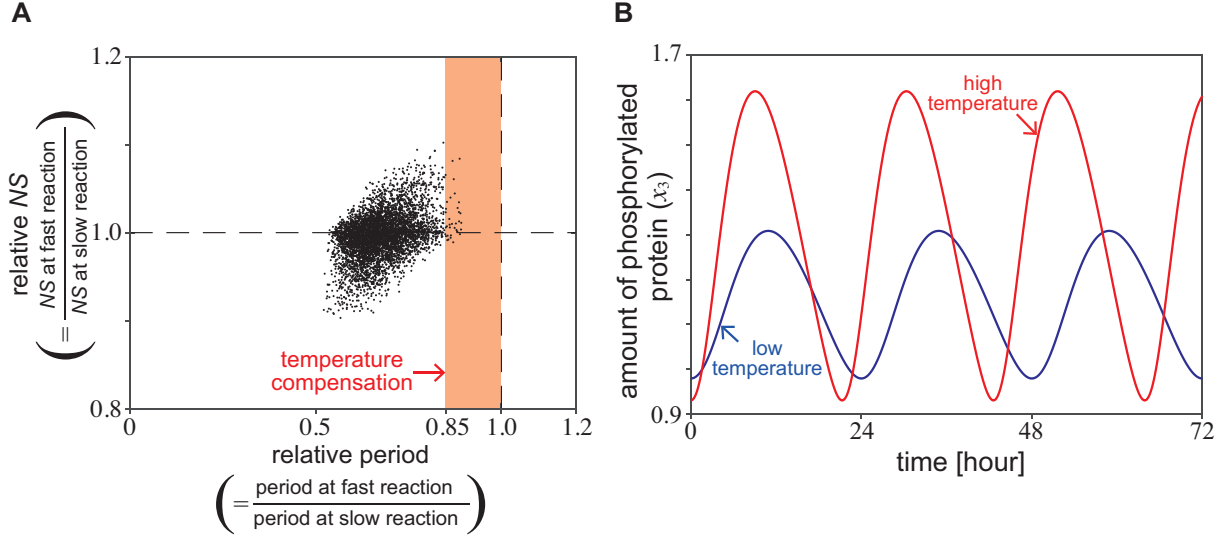


Figure 2: (A) Distribution of relative  $NS$  for  $x_3(t)$  of the circadian clock model as a function of the relative period when reaction rates are increased. We first generated reference parameter sets. To incorporate the effect of the increase of temperature, instead of using the Arrhenius equation, each parameter  $k_1$ ,  $k_2$ ,  $k_3$ ,  $p_1$ ,  $p_2$ , and  $r$  in the model's reference parameter set was randomly multiplied by a factor of 1.1-1.9. (B) Examples of the waveform in Goodwin model when the period was relatively unchanged. The blue and red lines represent slow and fast reactions, respectively.

### 3.2 RG analysis of waveform-period correlations

In the previous section, we demonstrated that the temperature compensation of the period in the Goodwin model is always accompanied by an increase of the index  $NS$  and waveform distortion correspondingly occurs as temperatures increase. This raises the following question: Is there a universal law governing the waveform distortion occurring when temperature increases? To answer this question, we derive an approximate solution for the time evolution of the Goodwin model for the circadian rhythm using a powerful reduction method, called "the renormalization-group(RG) method" [39]. The solution obtained using the RG method can be interpreted as the envelope of the set of solutions given in the perturbation theory, which has been applied to various models, including (but not limited to) ODE, PDE, discrete systems, and stochastic equations [41, 43, 53, 54, 60]. To apply the RG method, we again set the transcriptional regulation function  $f(x_3)$  to be  $r/x_3^n$ . In this function,  $n$  is the cooperativity of the transcriptional regulation, which is a Hopf bifurcation parameter. The approximate solution of the phosphorylated protein of the circadian clock reads (see Supplementary Information

A.2)

$$x_3(t) = \left( \frac{p_1 p_2 r}{s_3} \right)^{\frac{s_3}{s_1 s_2}} + \varepsilon A_0 \sin(\omega t) + \varepsilon^2 A_1 A_0^2 \sin(2\omega t + \alpha) + o(\varepsilon^2) \quad (7)$$

where we have

$$\varepsilon = n - \frac{s_4}{s_3}, \quad (8)$$

$$s_1 = k_1 + k_2 + k_3, \quad s_2 = k_1 k_2 + k_2 k_3 + k_3 k_1, \quad (9)$$

$$s_3 = k_1 k_2 k_3, \quad s_4 = (k_1 + k_2)(k_2 + k_3)(k_3 + k_1), \quad (10)$$

with the angular velocity and the phase parameter of the second-order term

$$\omega = \sqrt{s_2} - \varepsilon \frac{s_1 s_3 s_4}{6(2s_1 s_2^2 - (s_1^2 + 6s_2)s_3)\sqrt{s_2}} + o(\varepsilon^2), \quad (11)$$

$$\alpha = \arctan \left( \frac{s_1}{2\sqrt{s_2}} \right), \quad (12)$$

as well as the amplitudes

$$A_0 = \sqrt{\frac{4((s_1^2 + s_2)^2 - 2\varepsilon s_1 s_3)(s_1^2 + 4s_2)s_3^3}{\varepsilon(2s_1 s_2^2 - (s_1^2 + 6s_2)s_3)(s_1^2 + s_2)^2 s_4 s_1 s_2}} \left( \frac{p_1 p_2 r}{s_3} \right)^{\frac{s_3}{s_1 s_2}}, \quad (13)$$

$$A_1 = \frac{s_4 s_1}{12s_3 \sqrt{s_1^2 + 4s_2}} \left( \frac{s_3}{p_1 p_2 r} \right)^{\frac{s_3}{s_1 s_2}}. \quad (14)$$

The RG method provides an approximate but globally valid solution, and thus enable us to make a detailed investigation of the waveform distortion when temperature compensation occurs in the Goodwin model. The numerical analysis using the same parameter sets as used in Fig. 2A, in which the relative period in the model remains stable and within the interval (0.85, 1.0) against the temperature variations, shows that the phase parameter  $\alpha$  in the 2nd-order frequency tends to decrease with increasing reaction rates (see Fig. 3A). When the increase in reaction rates is small, the change in the phase of the second-order frequency scatters around zero and is negligible. However, with a significant increase in the reaction rates, the phase of the second order always tends to decrease as the reaction rates increase.

The significance of the phase parameter  $\alpha$  given in the second-order term on the waveform of the time series can be understood intuitively as follows: when the phase  $\alpha$  is large, the increasing

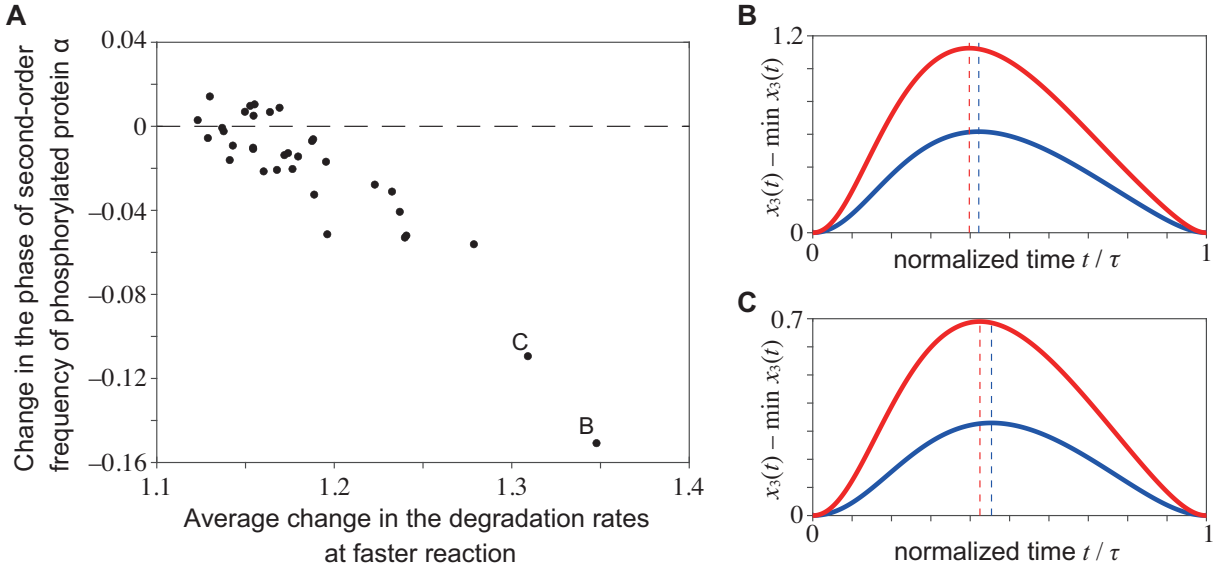


Figure 3: Change in the phase of the second-order frequency  $\alpha$  in phosphorylated protein oscillation under varying circadian clock model parameters. (A) The parameters  $k_1$ ,  $k_2$ ,  $k_3$ ,  $p_1$ ,  $p_2$ , and  $r$  were randomly increased from 1.1 to 1.9. The horizontal axis represents the arithmetic mean of the fast-case values of  $k_1$ ,  $k_2$ , and  $k_3$  divided by the slow-case values. The parameters  $p_1$ ,  $p_2$ , and  $r$  are omitted because they do not affect the period in Eq. (11). The vertical axis presents changes in the phase of the second-order frequency obtained via generalized harmonic analysis of numerically calculated periodic time series. When the period length is maintained (relative period within 0.85-1.0), the phase of  $\alpha$  of  $x_3(t)$  tends to decrease as the reaction rate increases. (B, C) Time series for the increased reaction rates (1.1-1.9) while maintaining the period. The red and blue lines represent the time series for increased reaction rates and those for the reference parameter set, respectively. The parameter values are provided in Supplementary Table 3. For comparison, the period length is standardized to 1. The time of the minimum value is set to 0, and the maximum phosphorylated protein oscillation is indicated by the dotted line. Increased reaction rates tend to advance the timing of the maximum oscillation.

duration tends to become longer because of the less overlap of the time profiles given by  $\sin(\omega t)$  and  $\sin(2\omega t + \alpha)$  (Fig. 3BC, blue line). Conversely, a smaller  $\alpha$  tends to result in a shorter increasing duration because of an additive effect of the two terms, which leads to a steeper slope on total, as presented in Fig. 3BC, red line. Therefore, the numerical results in Fig. 3A suggest that the decreasing duration of the time series elongates with as the reaction rate increases when the period is relatively stable despite the increasing reaction rate.

For a theoretical confirmation of the numerical result that the phase parameter  $\alpha$  given in the second-order term tends to become smaller as the temperature increases when the period is temperature-compensated, we analyze the sensitivity of the angular frequency  $\omega$  and the phase  $\alpha$  to the reaction rates by utilizing the results of the RG method. With use of Eqs. (11) and (12), we calculate  $d\omega = (\partial\omega/\partial k_1)dk_1 + (\partial\omega/\partial k_2)dk_2 + (\partial\omega/\partial k_3)dk_3$  and  $d\alpha = (\partial\alpha/\partial k_1)dk_1 + (\partial\alpha/\partial k_2)dk_2 + (\partial\alpha/\partial k_3)dk_3$ . In Fig. 4A, we present the parameter regions

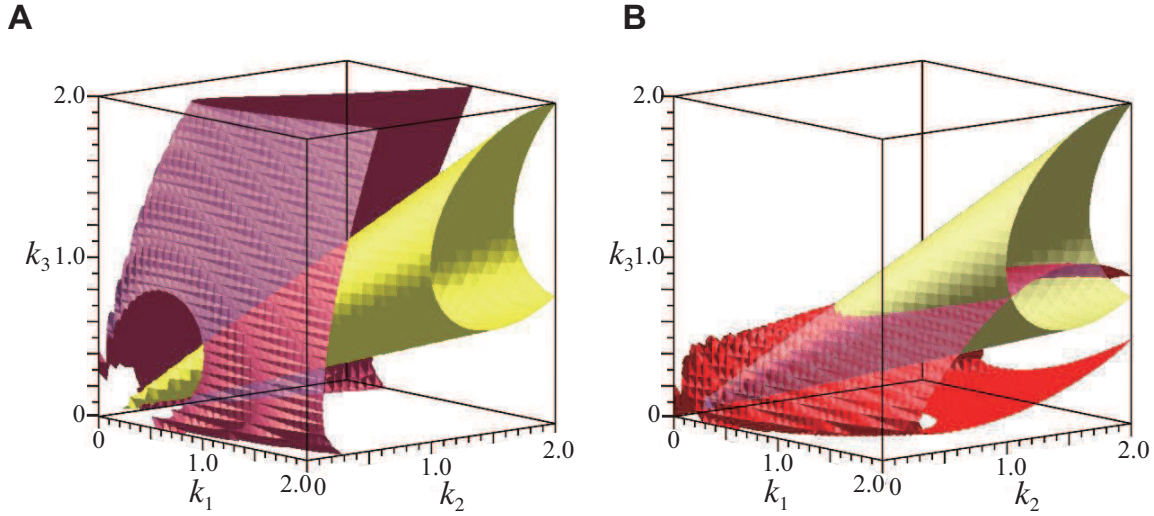


Figure 4: The parameter space for the constant period ( $d\omega = 0$ , red surface) with increasing degradation rates  $k_1$ ,  $k_2$ , and  $k_3$ , and that for the constant phase of second-order frequency ( $d\alpha = 0$ , yellow surface). The phase of second-order frequency  $\alpha$  should decrease with increasing  $k_1$ ,  $k_2$ , and  $k_3$  outside the yellow surface ( $d\alpha < 0$ ). The cooperativity  $n$  is  $n = 12$  (A), and  $n = 20$  (B), and the variations of the parameters are set to  $dk_1 = 0.3$ ,  $dk_2 = 0.2$ , and  $dk_3 = 0.1$ . (A) When  $n$  is small ( $n = 12$ ), surface  $d\omega = 0$  is included in space  $d\alpha < 0$ , which means that  $\alpha$  should become smaller if  $\omega$  does not change with increasing  $k_1$ ,  $k_2$ , and  $k_3$ . (B) When  $n$  is large ( $n = 20$ ), surface  $d\omega = 0$  can intersect  $d\alpha = 0$  although high cooperativity is unrealistic.

given by the constraints  $d\omega = 0$  (red surface) and  $d\alpha = 0$  (yellow surface) for the cooperativity  $n = 12$  of the transcription regulation. We can see that the region for  $d\alpha < 0$  (outside yellow surface) includes that given by the constraint  $d\omega = 0$  for all  $k_i$  ( $i = 1, 2, 3$ ). This implies that if the period is robust against a change in the parameters  $k_i$  ( $i = 1, 2, 3$ ), then the phase  $\alpha$  in the second-order term always becomes smaller with increasing parameters.

Next, let us examine how the parameter regions given by the constraints  $d\omega = 0$  and  $d\alpha = 0$  change with variations of the cooperativity  $n$ . The numerical calculation shows that the region corresponding to  $d\alpha < 0$  includes that given by  $d\omega = 0$  for  $n = 13$  and  $14$ . However, in the case of an exceedingly high cooperativity of transcription regulation  $n$ , which is not biologically realistic,  $d\alpha$  can be positive when  $d\omega = 0$ . For instance, for  $n = 20$ , although  $d\alpha$  is negative for most of the parameter space, there is a region in which  $d\alpha > 0$  when  $d\omega = 0$  (see Fig. 4B). These results indicate that if circadian rhythms are stable under temperature variations, the slope in the increasing phase of phosphoproteins should become sharper as temperature increases. Thus, we conclude that (i) the waveform of the gene activity rhythm should be

more distorted at higher temperatures, and (ii) the rate of the increase in phosphoprotein levels should be greater at higher temperatures if temperature compensation is achieved. In principle, these features can be tested experimentally.

### 3.3 Verification of the theoretical analysis of temperature compensation using published experimental data

The period formula Eq. (5) of the Goodwin model indicates that the non-sinusoidal index  $NS$  of the waveform of the circadian rhythms becomes larger, implying greater distortion of the waveform when all reactions are faster at higher temperatures during temperature compensation. To test this theoretical prediction of circadian gene activity in actual organisms, we analyze the waveform of the activity rhythms of the timeless gene in *Drosophila* at 18 and 29°C using published experimental data [55].

First, we extract the time series of the average curve from Fig. 3C in a prior study [55] using WebPlotDigitizer per hour. Second, we add uniformly distributed noise between  $-0.4$  and  $0.4$  to the extracted data to consider data errors. Then, we interpolate the time series every 0.1 h using spline interpolation (Fig. 5A). The interpolated data were detrended by multiplying an exponential function so that the position of the local minima of the oscillations are approximately reproduced. Then, the detrended time series is fitted with a sum of trigonometric functions up to the third harmonics using the generalized harmonic analysis (GHA) method [31, 61, 62, 63]. The width of the window for the analysis is set to one period. Using the Fourier coefficients of the fitting time series, we evaluate the distribution and average value of  $NS$ . The resultant  $NS$  of the activity rhythms of the timeless gene, as defined by Eq. (1), at a higher temperature (29 °C) tend to be larger than that at a lower temperature (18 °C), whereas the  $NS$  values are somewhat varied (Fig. 5B), which is consistent with the prediction. Experimental studies have demonstrated that temperature compensation can be impaired by genetic mutations. In the *Drosophila* mutant *perL*, the period increases with increasing temperature [55, 64]. Equation (5) implies that if the period increases with temperature, then the waveform of the circadian rhythm should be non-sinusoidal and more distorted at higher temperatures. Thus, it is predicted that the waveform of the circadian gene activity in *perL* should become more non-sinusoidal with higher temperatures. Again, we can quantify the waveform of *perL* using experimental data [55] (Supplementary Fig. 3). The waveform of circadian gene activity

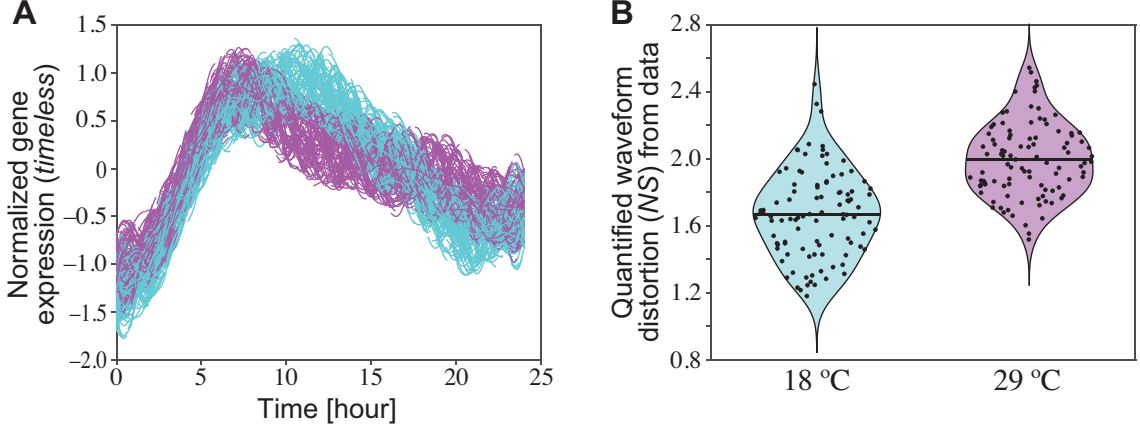


Figure 5: Analysis of the circadian waveform of wild-type *Drosophila* at different temperatures using previously reported experimental data [55]. (A) Re-plot of Fig. 3C in [55]. The average curves of *tim-luc* at 18 and 29 °C are extracted, and uniformly distributed noise between  $-0.4$  and  $0.4$  is added to the extracted data, generating 100 time series datasets. Spline interpolation is applied to set the sampling interval to  $0.1$  h. The interpolated time series data at 18 (cyan) and 29 °C (magenta) are plotted. (B) Distribution of the quantified waveform distortion ( $NS$ ) from the data at 18 (cyan) and 29 °C (magenta). The time series data with noise are detrended by multiplying an exponential function so that the positions of local minima of the oscillations are approximately equal. The Fourier coefficients of the detrended time series are quantified using GHA. The  $NS$  values are estimated from the coefficients up to the third harmonics. Dots represent the  $NS$  values for each dataset, and the horizontal lines represent their average values.

tends to be more non-sinusoidal at higher temperatures in perL, as observed in the wild-type, whereas the  $NS$  values varied, in line with the prediction.

## 4 Theoretical analysis of synchronization in the circadian rhythm model

The numerical result in Fig. 1B shows that the range of synchronization into the light-dark cycles tends to decrease as the waveform becomes more distorted in the simple circadian clock model. To clarify the condition for synchronization, we again consider the Goodwin model but with an external force incorporated as follows:

$$\frac{dx_1}{dt} = f(x_3) - k_1x_1 + I \cos(\Omega t) \quad (15)$$

$$\frac{dx_2}{dt} = p_1x_1 - k_2x_2 \quad (16)$$

$$\frac{dx_3}{dt} = p_2x_2 - k_3x_3 \quad (17)$$

where  $I \cos(\Omega t)$  is a periodic environmental change, such as a light-dark cycle. By eliminating  $x_1$  and  $x_2$ , Eqs. (15)-(17) is converted to the following single equation:

$$\frac{d^3 x_3}{dt^3} + s_1 \frac{d^2 x_3}{dt^2} + s_2 \frac{dx_3}{dt} + s_3 x_3 = p_1 p_2 f(x) + p_1 p_2 I \cos(\Omega t). \quad (18)$$

If the model is to admit a synchronization to the external cycle  $I \cos(\Omega t)$  at all, then  $x_3(t)$  should be written as the Fourier series  $x_3(t) = \sum_{j=-\infty}^{\infty} a_j \exp(i\Omega j t)$ . Multiplying Eq. (18) by  $dx/dt$  and integrating that for the interval  $t$  to  $t + 2\pi/\Omega$ , we have the following equation:

$$\Omega^3 - \omega^2 \Omega = \frac{1}{2} p_1 p_2 I \mathcal{R} \sin \beta \quad (19)$$

where

$$\omega = 2\pi/\tau = \sqrt{s_2 \frac{\sum_{j=1}^{\infty} |a_j|^2 j^2}{\sum_{j=1}^{\infty} |a_j|^2 j^4}}$$

is the natural angular frequency without the external force and

$$\mathcal{R} = \frac{|a_1|}{\sum_{j=1}^{\infty} |a_j|^2 j^4} \quad (20)$$

with  $\beta$  being the argument of  $a_1$  such that  $a_1 = |a_1| \exp(i\beta)$ . Because  $-1 \leq \sin \beta \leq 1$ , when  $x(t)$  synchronizes with the external cycles, the angular frequency of the external cycles ( $\Omega$ ) should satisfy the inequality

$$|\Omega^3 - \omega^2 \Omega| \leq \frac{1}{2} p_1 p_2 I \mathcal{R}. \quad (21)$$

We note that  $\mathcal{R}$  defined by Eq. (20) becomes smaller when the components of higher harmonics become larger and the waveform exhibits greater distortion. Therefore, if the waveform is more distorted by, say, an increasing temperature, the bounds of Eq. (21) become smaller, and accordingly, the allowed region of the middle term is narrower. The left hand side of Eq. (21) is a cubic function of  $\Omega$ , which is monotonically increasing near  $\Omega = \omega$ . If the waveform is more distorted, Eq.(20) should be smaller, making the allowed region of Eq. (21) narrower. Then, the range of  $\Omega$  that causes synchronization becomes narrower, as presented in Fig. 6. This indicates that the range of synchronization into light-dark cycles always decreases as the waveform becomes more distorted in the simple circadian model, which is consistent with the

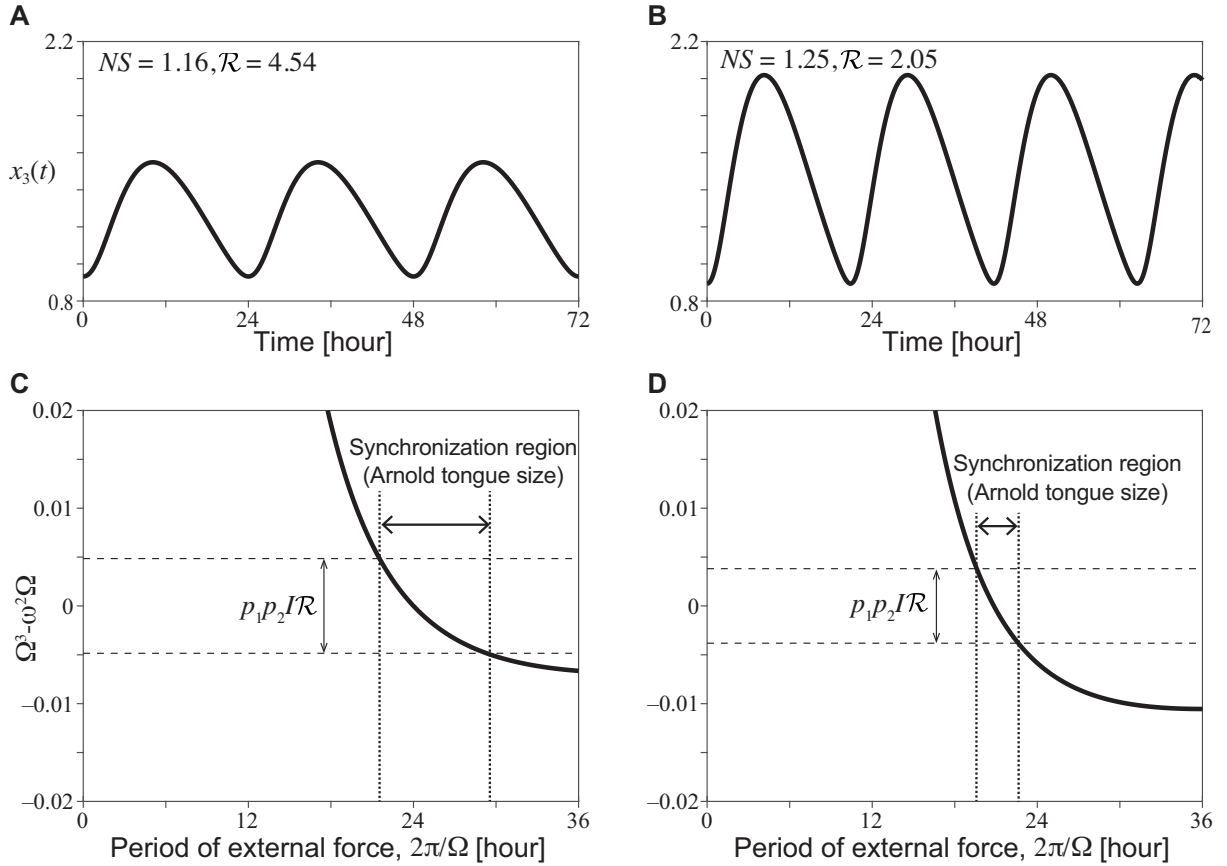


Figure 6: The time series depicts cases in which the period length remains relatively constant despite increasing reaction rates in the circadian clock model (A: reference set case, B: increased reaction rates case). Additionally, synchronization regions for these cases are presented (C: reference set case, D: increased reaction rates case). Panels A and B correspond to Fig. 3B, but they include additional waveform values such as  $NS$  and  $\mathcal{R}$ . Synchronization regions for  $I = 0.03$  in Eq. (15) (C, D), calculated using Eq. (21), are illustrated for each oscillation (A and B). Synchronization with the external forcing period occurs only when the cubic function  $\Omega^3 - \omega^2\Omega$  falls within a specific range. This range becomes narrower as the waveform distortion increases along with reaction rates, consistent with the observations in Fig. 1B.

numerical simulation in Fig. 1B.

## 5 Discussion

We theoretically explored the conditions for clarifying the temperature compensation of the biological clock and its synchronization to light-dark cycles with a particular focus on waveform distortion. The theoretical analysis of the Goodwin model, one of the most studied models of biological clocks, revealed that waveform distortion of gene activity rhythms with increasing temperature is necessary for temperature compensation. Furthermore, we derived an approximate but globally valid solution to the waveform of the time profiles using the RG method



as a powerful tool for global analysis. This allowed us to investigate, based on the analytical solution, whether there is a universal law for the mechanism by which the waveform changes with temperature variation.

The results indicated that temperature compensation is more likely to occur if the waveform is distorted if the decreasing duration of circadian protein oscillation elongates as temperature increases. Although theoretical predictions based on a model might not always be realized in real organisms, we quantified the gene activity rhythms of published experimental data using *Drosophila*. This quantification confirmed that the waveform is distorted at high temperatures, in accordance with our theoretical predictions.

It is notable that the systematic wave distortion governed by Eq. (5), which we have found to hold in the Goodwin model, also applies to a wide class of non-linear oscillators used for biological phenomena different from biological rhythms, including the Lotka-Volterra model [65], which is commonly used in ecology, and the van der Pol model, as presented in the Supplementary Information A.3 and A.4 (see also [31]). This suggests that exploring the possible significance of waveform distortion in other mathematical models, such as the Fitz-Hugh-Nagumo model in neuroscience, would be intriguing [65, 66, 67].

To the best of our knowledge, this is the first study to apply the RG method, a powerful resummation method of the perturbation series first developed in physics, to circadian rhythm problems. In the RG method, secular terms appearing in the naïve perturbation series are renormalized into the 'integral constants', which thus acquire the nature of the slow modes, making it a powerful tool for global and asymptotic analysis. Unlike the naive perturbation theory, the solutions given by the RG method provide a time evolution close to numerical simulations in the relevant global domain of time, offering an approximate solution for the period and waveform. The analytical results predict that longer tails of gene activity rhythms at higher temperatures occur for temperature compensation.

This study also investigated the synchronization with environmental light-dark cycles at various temperatures [33, 34]. The numerical simulations and theoretical analysis predict that as the distortion of the gene activity rhythms for achieving a temperature-compensated period increases, it becomes more difficult to synchronize with the light-dark cycle. This prediction aligns with the reported temperature-dependent variation in response to light pulses in *Drosophila* and *Neurospora*, displaying smaller phase shifts at higher temperatures [56] [57].

As mentioned in the Introduction, previous theoretical and experimental studies, such as those using *Drosophila* [55], suggested that waveforms in gene activity rhythms do not change under temperature variations, although they are blurred by error bands. These findings are apparently inconsistent with our current conclusion. We believe that this discrepancy stems from two main factors: differing assumptions about the temperature sensitivity of degradation rates and differing interpretations of experimental results regarding gene activity rhythms at distinct temperatures. First, the previous study assumed that all degradation rates are temperature-insensitive. Thus, the waveform of gene activity rhythms does not need to change with temperature. By contrast, we assume that some degradation rates at least should accelerate with temperature, leading to a more distorted waveform of gene activity rhythms at higher temperatures. Second, the previous study [55] interpreted their experimental results as indicating that gene activity rhythms at different temperatures can be collapsed onto each other by rescaling, supporting their prediction that temperature compensation occurs because of rescaling and the stability of the temperature insensitivity of degradation rates. Conversely, our quantification of their experimental data indicated that the waveform tends to be more distorted at higher temperatures, whereas variation in  $NS$  values was noted. Thus, the present result is consistent with our theoretical prediction. We believe that further systematic quantification of the waveforms of gene activity and/or protein activity rhythms in various circadian organisms will be essential for clarifying the importance of the waveform in circadian rhythms in the future.

## Methods

### Computation of ODEs

The ordinary differential equations in this work were calculated by a fourth-order Runge-Kutta method with MATLAB (The MathWorks, Natick, MA). The time step size  $\Delta t$  for the Goodwin model (Eqs. (2)-(4)) was 0.001, and that for the Lotka-Volterra model (Eqs. (98)-(99)) and the van der Pol oscillator (Eq. (108)) was 0.0001.

### Numerical analysis of synchronization with light-dark cycles

The angular frequency of the light-dark cycle  $\Omega$  in Eq. (6) was changed by 0.0001. We considered that the model was synchronized with the light-dark cycle when the change in the amplitude was smaller than the rounding error as in Fig. 1B.

## Estimation of waveform distortion from simulated time-series

We estimated waveform distortion, i.e., non-sinusoidal power ( $NS$ , see Eq. (1)) from the simulated time-series by using the generalized harmonic analysis (GHA) method as in Figs. 1B and 2A. The GHA method estimates the amplitudes  $A_j$  and  $B_j$ , and the frequencies  $f_j$ , which minimize the squared residual  $\int_0^L [x(t) - \sum_{j=1}^{j^{max}} \{A_j \cos(2\pi f_j t) + B_j \sin(2\pi f_j t)\}]^2 dt$ . The detailed procedure of GHA can be found in [31, 62].

## Estimation of phases of Fourier components from simulated time-series

By using GHA method, we computed the Fourier series  $x(t) = \sum_{j=1}^{j^{max}} \{A_j \cos(2\pi f_j t) + B_j \sin(2\pi f_j t)\}$ . This form was converted into  $x(t) = \sum_{j=1}^{j^{max}} r_j \sin(2\pi f_j t + \alpha_j)$ , where  $r_j = \sqrt{A_j^2 + B_j^2}$  and  $\alpha_j = \arctan(B/A)$ .

## Computation of parameter space for temperature compensation using the RG method

The frequency change  $d\omega = (\partial\omega/\partial k_1)dk_1 + (\partial\omega/\partial k_2)dk_2 + (\partial\omega/\partial k_3)dk_3$  and the phase change  $d\alpha = (\partial\alpha/\partial k_1)dk_1 + (\partial\alpha/\partial k_2)dk_2 + (\partial\alpha/\partial k_3)dk_3$  were calculated from Eqs. (11) and (12) by using Maple. The parameter space for  $d\omega = 0$  and  $d\alpha = 0$  in Fig. 4AB were numerically generated by Maple.

## Estimation of waveform distortion from published experimental data

The average curves of experimental time-series of *timeless* luciferase (*tim-luc*) reporter (shown to recapitulate the dynamics of *timeless* gene expression) at 18 and 29 °C of Figs. 3C and 4B in the published literature [55] were extracted using WebPlotDigitizer at 1 h intervals. Uniformly distributed noise between  $-0.4$  and  $0.4$  was added to the extracted data, generating 100 time series datasets so that the experimental noise is roughly reproduced as in Fig. 5A and Supplementary Fig. 3A. Spline interpolation was applied to set the sampling interval to 0.1 h to smooth time series data. The time series data with noise were detrended by multiplying an exponential function so that the positions of local minima of the oscillations are approximately reproduced. The Fourier coefficients of the detrended time series were quantified using GHA. The  $NS$  values were estimated from the coefficients up to the third harmonics as in Fig. 5B and Supplementary Fig. 3B.

## Acknowledgements

We thank H. Nakao, H. Chiba, Y. Kawahara, A. Mochizuki for useful comments on this study. This work was supported by grants from Japan Science and Technology Agency (JPMJCR1913 to G.K.), and from the Japanese Society for the Promotion of Science, and the Ministry of Education, Culture, Sports, Science, and Technology in Japan (JP21K06105 to G.K., 19K03872 to T.K.).

## References

- [1] Jay C Dunlap. Molecular bases for circadian clocks. Cell, 96:271–290, 1999.
- [2] Stacey L Harmer, Satchidananda Panda, and Steve A Kay. Molecular Bases of Circadian Rhythms. Annua Rev Cell Dev Biol, 17:215–253, 2001.
- [3] Rachel S. Edgar, Edward W. Green, Yuwei Zhao, Gerben van Ooijen, Maria Olmedo, Ximing Qin, Yao Xu, Min Pan, Utham K. Valekunja, Kevin A. Feeney, Elizabeth S. Maywood, Michael H. Hastings, Nitin S. Baliga, Martha Merrow, Andrew J. Millar, Carl H. Johnson, Charalambos P. Kyriacou, John S. O’Neill, and Akhilesh B. Reddy. Peroxiredoxins are conserved markers of circadian rhythms. Nature, 485:459–464, 2012.
- [4] Paul E. Hardin, Jeffrey C. Hall, and Michael Rosbash. Feedback of the *Drosophila* period gene product on circadian cycling of its messenger RNA levels. Nature, 343:536–540, 1990.
- [5] Caroline H Ko and Joseph S Takahashi. Molecular components of the mammalian circadian clock. Hum. Mol. Genet., 15:R271–7, 2006.
- [6] Trey K Sato, Rikuhiko G Yamada, Hideki Ukai, Julie E Baggs, Loren J Miraglia, Tetsuya J Kobayashi, David K Welsh, Steve A Kay, Hiroki R Ueda, and John B Hogenesch. Feedback repression is required for mammalian circadian clock function. Nat Genet, 38:312–9, 2006.
- [7] Jeanne F Duffy and Kenneth P Wright Jr. Entrainment of the human circadian system by light. J. Biol. Rhythm., 20:326–338, 2005.
- [8] Kong L Toh, Christopher R Jones, Yan He, Erik J Eide, William A Hinz, David M Virshup, Louis J Ptáček, and Ying-Hui Fu. An hPer2 phosphorylation site mutation in familial advanced sleep phase syndrome. Science, 291:1040–3, 2001.
- [9] Katja Vanselow, Jens T Vanselow, Pål O Westermark, Silke Reischl, Bert Maier, Thomas

- Korte, Andreas Herrmann, Hanspeter Herzog, Andreas Schöller, and Achim Kramer. Differential effects of PER2 phosphorylation: molecular basis for the human familial advanced sleep phase syndrome (FASPS). Genes Dev., 20:2660–2672, 2006.
- [10] Y Xu, K L Toh, C R Jones, J-Y Shin, Y-H Fu, and L J Ptáček. Modeling of a Human Circadian Mutation Yields Insights into Clock Regulation by PER2. Cell, 2007.
- [11] Steven A Brown, Dieter Kunz, Amelie Dumas, Pål O Westermark, Katja Vanselow, Amely Tilmann-Wahnschaffe, Hanspeter Herzog, and Achim Kramer. Molecular insights into human daily behavior. Proc. Natl. Acad. Sci. USA, 105:1602–1607, 2008.
- [12] Adrián E Granada, Grigory Bordyugov, Achim Kramer, and Hanspeter Herzog. Human Chronotypes from a Theoretical Perspective. PLoS ONE, 2013.
- [13] Jean-Michel Fustin, Rika Kojima, Kakeru Itoh, Hsin-Yi Chang, Shiqi Ye, Bowen Zhuang, Asami Oji, Shingo Gibo, Rajesh Narasimamurthy, David Virshup, Gen Kurosawa, Masao Doi, Ichiro Manabe, Yasushi Ishihama, Masahito Ikawa, and Hitoshi Okamura. Two Ck1δ transcripts regulated by m6A methylation code for two antagonistic kinases in the control of the circadian clock. Proc. Natl. Acad. Sci. USA, 115:5980–5985, 2018.
- [14] Youna Hu, Alena Shmygelska, David Tran, Nicholas Eriksson, Joyce Y. Tung, and David A Hinds. GWAS of 89,283 individuals identifies genetic variants associated with self-reporting of being a morning person. Nature Communications, 2016.
- [15] Jacqueline M Lane, Irma Vlasac, Simon G Anderson, Simon D Kyle, William G Dixon, David A Bechtold, Shubhroz Gill, Max A Little, Annemarie Luik, Andrew Loudon, Richard Emsley, Frank A J L Scheer, Deborah A Lawlor, Susan Redline, David W Ray, Martin K Rutter, and Richa Saxena. Genome-wide association analysis identifies novel loci for chronotype in 100,420 individuals from the UK Biobank. Nature Communications, 2016.
- [16] Guangsen Shi, David Wu, Louis J Ptáček, and Ying-Hui Fu. Human genetics and sleep behavior. Current Opinion in Neurobiology, 2017.
- [17] Woodland J. Hastings and Beatrice M. Sweeney. On the mechanism of temperature independence in a biological clock. Proc. Natl. Acad. Sci. USA, 43:804–811, 1957.
- [18] Peter Ruoff. Introducing temperature-compensation in any reaction kinetic oscillator model. Journal of Interdisciplinary Cycle Research, 1992.

- [19] Norman F Ruby, D Erik Burns, and H Craig Heller. Circadian rhythms in the suprachiasmatic nucleus are temperature-compensated and phase-shifted by heat pulses in vitro. Journal of Neuroscience, 1999.
- [20] Tetsuhiro S Hatakeyama and Kunihiro Kaneko. Reciprocity Between Robustness of Period and Plasticity of Phase in Biological Clocks. Phys. Rev. Lett., 115:218101, 2015.
- [21] Min Zhou, Jae Kyoung Kim, Gracie Wee Ling Eng, Daniel B Forger, and David M Virshup. A period2 phosphoswitch regulates and temperature compensates circadian period. Mol. Cell, 60:77–88, 2015.
- [22] Gen Kurosawa, Atsuko Fujioka, Satoshi Koinuma, Atsushi Mochizuki, and Yasufumi Shigeyoshi. Temperature–amplitude coupling for stable biological rhythms at different temperatures. PLoS Computational Biology, 2017.
- [23] Masaki Sasai. Role of the reaction-structure coupling in temperature compensation of the KaiABC circadian rhythm. PLoS Computational Biology, 2022.
- [24] Christoph Schmal, Bert Maier, Reut Ashwal-Fluss, Osnat Bartok, Anna-Marie Finger, Tanja Bange, Stella Koutsouli, Maria S Robles, Sebastian Kadener, Hanspeter Herzog, and Achim Kramer. Alternative polyadenylation factor CPSF6 regulates temperature compensation of the mammalian circadian clock. PLoS Biology, 2023.
- [25] Suchana Chakravarty, Christian I Hong, and Attila Csikász-Nagy. Systematic analysis of negative and positive feedback loops for robustness and temperature compensation in circadian rhythms. npj Systems Biology and Applications volume, 2023.
- [26] Gen Kurosawa and Yoh Iwasa. Temperature compensation in circadian clock models. J. Theor. Biol., 233:453–468, 2005.
- [27] Kazuki Terauchi, Yohko Kitayama, Taeko Nishiwaki, Kumiko Miwa, Yoriko Murayama, Tokitaka Oyama, and Takao Kondo. ATPase activity of KaiC determines the basic timing for circadian clock of cyanobacteria. Proc. Natl. Acad. Sci. USA, 2007.
- [28] C I Hong, E D Conrad, and J J Tyson. A proposal for robust temperature compensation of circadian rhythms. Proc. Natl. Acad. Sci. USA, 2009.
- [29] Yasushi Isojima, Masato Nakajima, Hideki Ukai, Hiroshi Fujishima, Rikuhiko G Yamada, Koh hei Masumoto, Reiko Kiuchi, Mayumi Ishida, Maki Ukai-Tadenuma, Yoichi Mi-

- namo, Ryotaku Kito, Kazuki Nakao, Wataru Kishimoto, Seung-Hee Yoo, Kazuhiro Shimomura, Toshifumi Takao, Atsuko Takano, Toshio Kojima, Katsuya Nagai, Yoshiyuki Sakaki, Joseph S Takahashi, and Hiroki R. Ueda.  $CKI\delta/\varepsilon$ -dependent phosphorylation is a temperature-insensitive, period-determining process in the mammalian circadian clock. Proc. Natl. Acad. Sci. USA, 2009.
- [30] Patricia L. Lakin-Thomas, Stuart Brody, and Gary G. Coté. Amplitude model for the effects of mutations and temperature on period and phase resetting of the *Neurospora* circadian oscillator. J. Biol. Rhythms, 6:281–297, 1991.
- [31] Shingo Gibo and Gen Kurosawa. Non-sinusoidal waveform in temperature-compensated circadian oscillations. Biophys. J., 116:741–751, 2019.
- [32] Steven H. Strogatz. Nonlinear dynamics and chaos: with applications to physics, biology, chemistry, and engineering (studies in nonlinearity). CRC Press, 2015.
- [33] A Pikovsky, M Rosenblum, and J Kurths. Synchronization: A Universal Concept in Nonlinear Sciences. Cambridge University Press, 2003.
- [34] U Abraham, A E Granada, P O Westermark, M Heine, A Kramer, and H Herzl. Coupling governs entrainment range of circadian clocks. Molecular Systems Biology, 2010.
- [35] A E Granada, T Cambras, A Díez-Noguera, and H Herzl. Circadian desynchronization. Interface Focus, 1:153–166, 2011.
- [36] S K Crosthwaite, J J Loros, and J C Dunlap. Light-induced resetting of a circadian clock is mediated by a rapid increase in frequency transcript. Cell, 81:1003–1012, 1995.
- [37] Y Shigeyoshi, K Taguchi, S Yamamoto, S Takekida, L Yan, H Tei, T Moriya, S Shibata, J J Loros, and J C Dunlap H Okamura. Light-induced resetting of a mammalian circadian clock is associated with rapid induction of the *mPer1* transcript. Cell, 91:1043–1053, 1997.
- [38] Tsutomu Takeuchi, Takamichi Hinohara, Gen Kurosawa, and Kenko Uchida. A temperature-compensated model for circadian rhythms that can be entrained by temperature cycles. J. Theor. Biol., 246:195–204, 2007.
- [39] Nigel Goldenfeld, Olivier Martin, and Yoshitsugu Oono. Intermediate asymptotics and renormalization group theory. Journal of Scientific Computing, 4:355–372, 1989.

- [40] Lin Y. Chen, Nigel Goldenfeld, and Yoshitsugu Oono. Renormalization group theory for global asymptotic analysis. Phys. Rev. Lett., 73:1311–1315, 1994.
- [41] Teiji Kunihiro. A geometrical formulation of the Renormalization group method for global analysis. Prog. Theor. Phys., 94:503–514, 1995.
- [42] Robert Graham. Systematic derivation of a rotationally covariant extension of the two-dimensional Newell-Whitehead-Segel equation. Phys. Rev. Lett., 76:2185–2187, 1996.
- [43] Teiji Kunihiro. The renormalization-group method applied to asymptotic analysis of vector fields. Prog. Theor. Phys., 97:179–200, 1997.
- [44] Teiji Kunihiro. A geometrical formulation of the renormalization group method for global analysis II: Partial differential equations. Prog. Theor. Phys., 14:51–69, 1997.
- [45] ShinIchi Sasa. Renormalization group derivation of phase equations. Physica D, 108:45–59, 1997.
- [46] Tsuyoshi Maruo, Kazuhiro Nozaki, and Akira Yosimori. Derivation of the Kuramoto-Sivashinsky equation using the renormalization group method. Prog. Theor. Phys., 101:243–249, 1999.
- [47] John Veysey and Nigel Goldenfeld. Simple viscous flows: From boundary layers to the renormalization group. Rev. Mod. Phys., 79:883–925, 2007.
- [48] R.E. Lee DeVille, Anthony Harkin, Matt Holzer, Krešimir Josić, and Tasso J. Kaper. Analysis of a renormalization group method and normal form theory for perturbed ordinary differential equations. Physica D, 237:1029–1052, 2008.
- [49] Hayato Chiba. Extension and unification of singular perturbation methods for ODEs based on the renormalization group method. SIAM. J. on Appl. Dyn. Syst., 8:1066–1115, 2009.
- [50] Jr Robert E. O’Malley and Eleftherios Kirkinis. A combined renormalization group-multiple scale method for singularly perturbed problems. Stud. Appl. Math., 124:383–410, 2010.
- [51] Yoshitsugu Oono. The nonlinear world: Conceptual analysis and phenomenology. Springer, 2012.
- [52] Matt Holzer and Tasso J. Kaper. An analysis of the renormalization group method for



- asymptotic expansions with logarithmic switchback terms. Adv. Differ. Equ., 19:245–282, 2014.
- [53] Shin-Ichiro Ei, Kazuyuki Fujii, and Teiji Kunihiro. Renormalization-group method for reduction of evolution equations; invariant manifolds and envelopes. Annals of Phys., 280:236–298, 2000.
- [54] Teiji Kunihiro, Yuta Kikuchi, and Kyosuke Tsumura. Geometrical Formulation of Renormalization-Group Method as an Asymptotic Analysis: With Applications to Derivation of Causal Fluid Dynamics. Springer-Verlag, 2022.
- [55] Philip B. Kidd, Michael W. Young, and Eric D. Siggia. Temperature compensation and temperature sensation in the circadian clock. Proc. Natl. Acad. Sci. USA, 112:E6284–E6292, 2015.
- [56] H Nakashima and J F Feldman. Temperature-sensitivity of light-induced phase shifting of the circadian clock of *Neurospora*. Photochem. Photobiol, 1980.
- [57] V Varma, N Mukherjee, N N Kannan, and VK Sharma. Strong (Type 0) Phase Resetting of Activity-Rest Rhythm in Fruit Flies, *Drosophila Melanogaster*, at Low Temperature. Journal of Biological Rhythms, 2013.
- [58] Brian C Goodwin. Oscillatory behavior in enzymatic control processes. Adv. Enzyme Regul., 3:425–538, 1965.
- [59] Daniel B. Forger. Signal processing in cellular clocks. Proc. Natl. Acad. Sci. USA, 108:4281–4285, 2011.
- [60] Teiji Kunihiro and Junta Matsukidaira. Dynamical reduction of discrete systems based on the renormalization-group method. Physical Review E, 57:4817–4820, 1998.
- [61] N Wiener. The Fourier integral and certain of its applications. Dover, 1958.
- [62] T Terada, H Nakajima, M Tohyama, and Y Hirata. Nonstationary waveform analysis and synthesis using generalized harmonic analysis. IEEE-SP International Symposium on Time-Frequency and Time-Scale Analysis, 1994.
- [63] Shingo Gibo and Gen Kurosawa. Theoretical study on the regulation of circadian rhythms by RNA methylation. J. Theor. Biol., 490:110140, 2020.

- [64] Z J Huang, K D Curtin, and M Rosbash. PER protein interactions and temperature compensation of a circadian clock in *Drosophila*. Science, 1995.
- [65] J D Murray. Mathematical Biology. Springer-Verlag, 1988.
- [66] R FitzHugh. Impulses and physiological states in theoretical models of nerve membrane. Biophysical J, 1961.
- [67] J Nagumo, S Arimoto, and S Yoshizawa. An active pulse transmission line simulating nerve axon. Proc IRE, 1962.
- [68] J. S. Frame. Explicit solutions in two species Volterra systems. J. Theor. Biol., 43:73–81, 1974.

## Supporting Information for

# Waveform distortion for temperature compensation and synchronization in circadian rhythms: An approach based on the renormalization group method

Shingo Gibo<sup>1\*</sup>, Teiji Kunihiro<sup>2</sup>, Tetsuo Hatsuda<sup>1</sup>, and Gen Kurosawa<sup>1\*</sup>

<sup>1</sup>Interdisciplinary Theoretical and Mathematical Sciences Program (iTHEMS), RIKEN

<sup>2</sup>Yukawa Institute for Theoretical Physics (YITP), Kyoto University

\*Correspondence: shingo.gibo@riken.jp (S.G), g.kurosawa@riken.jp (G.K)

### **This PDF includes:**

Supplementary Text

Supplementary Figures 1 to 3

Supplementary Tables 1 to 2

# Supplementary Text

## A.1 Brief introduction of the renormalization group (RG) method using a simple model with Hopf bifurcation

In this section, we introduce the RG method [39] in a geometrical manner as formulated in [41, 53] with a simpler prescription without the redundant 'time-splitting' procedure. In this aim, we use a generic model with a Hopf bifurcation. A more detailed account of the method is given in [54].

Let us consider the model equation

$$Lx(t) = F(x(t); \varepsilon) \quad (22)$$

where  $x(t)$  is a state variable of our dynamics,  $L = \sum_{n=1}^N a_n (d/dt)^n$  is a linear differential operator,  $F(x(t); \varepsilon)$  is a nonlinear function of  $x(t)$ , and  $\varepsilon$  is an internal parameter of  $F$ , which acts as a bifurcation parameter of the system. We assume that the model has a fixed point  $x_0$  satisfying the equation  $F(x_0; 0) = 0$ , which is destabilized for  $\varepsilon > 0$  through the Hopf bifurcation. We are interested in the derivation of the reduced equation and an approximate but valid solution in a global domain of time around the critical point of the Hopf bifurcation. Thus, we apply the perturbation theory and express the solution around an arbitrary time  $t = t_0$  belonging to a global domain in the asymptotic regime (see below) in a power series of  $\varepsilon$  as follows:

$$x(t; t_0) = x_0 + \varepsilon u_1(t; t_0) + \varepsilon^2 u_2(t; t_0) + \varepsilon^3 u_3(t; t_0) + o(\varepsilon^3). \quad (23)$$

Substituting Eq. (23) into Eq. (22) and equating the terms with the same powers of  $\varepsilon$ , we obtained

$$O(\varepsilon^1) : L'u_1 = 0, \quad (24)$$

$$O(\varepsilon^2) : L'u_2 = f_1(u_1), \quad (25)$$

$$O(\varepsilon^3) : L'u_3 = f_2(u_1, u_2), \quad (26)$$

where

$$L' = L - (\partial F / \partial x)|_{x=x_0, \varepsilon=0},$$

and  $f_1(u_1)$  and  $f_2(u_1, u_2)$  are nonlinear functions that depend on  $F(x_0)$ . Because Hopf bifurcation occurs at  $\varepsilon = 0$ , two of the eigenvalues of the linear differential operator  $L'$  are written as  $\pm i\omega_0$ , with  $\omega_0$  being a real number, and the others have negative real parts as  $Re(\lambda_k) < 0$  ( $k = 1, \dots, N - 2$ ).

Then, the first-order solution can be expressed as

$$u_1(t; t_0) = A(t_0) \cos(\omega_0 t + \theta(t_0)) + \sum_{k=1}^{N-2} c_k(t_0) e^{\lambda_k t}, \quad (27)$$

where  $A(t_0)$ ,  $\theta(t_0)$ , and  $c_k(t_0)$  are the integral constants which are assumed to depend on the initial time  $t_0$ .

Next, we consider the asymptotic regime as  $t \rightarrow \infty$  so that the second term describing the transient behavior has virtually become negligible. Then, the first-order solution in this asymptotic regime can be expressed only by the first term as

$$u_1(t \rightarrow \infty; t_0) = A(t_0) \cos(\omega_0 t + \theta(t_0)). \quad (28)$$

Next, we proceed to the second-order equation. Substituting Eq. (28) into Eq. (25), we have

$$L'u_2 = b_1 A \cos(\omega_0 t + \theta) + b_2 A^2 \cos(2(\omega_0 t + \theta)) + b_3 A^2, \quad (29)$$

where  $b_k$  ( $k = 1, 2$ ) are constants depending on  $f_1(u_1)$ . It is to be noted that the inhomogeneous part (r.h.s.) contains a term proportional to  $\cos(\omega_0 t + \theta)$ , which is a zero mode of the linear operator that gives rise to secular terms in the particular solutions of the inhomogeneous equation. The general solution to Eq. (29) is given as a sum of a particular solution to the inhomogeneous equation and the general solution to the homogeneous equation. Now, it is possible and convenient to choose the coefficients of the latter so that all of the secular terms vanish at  $t = t_0$  [41], which leads to the second-order solution as

$$\begin{aligned} u_2(t; t_0) = & (t - t_0)d_1 A \cos(\omega_0 t + \theta) + (t - t_0)d_2 A \sin(\omega_0 t + \theta) \\ & + d_3 A^2 \cos(2(\omega_0 t + \theta)) + d_4 A^2 \sin(2(\omega_0 t + \theta)) + d_5 A^2, \end{aligned} \quad (30)$$

where  $d_k$  ( $k = 1 \cdots 5$ ) are constants depending on the right-hand side of Eq. (29).

Similarly, the third-order solution takes the form of

$$\begin{aligned}
u_3(t; t_0) = & (t - t_0)(f_{1a}A^3 + f_{1b}A) \cos(\omega_0 t + \theta) + (t - t_0)(f_{2a}A^3 + f_{2b}A) \sin(\omega_0 t + \theta) \\
& + (t - t_0)^2 f_3 A \cos(\omega_0 t + \theta) + (t - t_0)^2 f_4 A \sin(\omega_0 t + \theta) + f_5 A^2 \cos(2(\omega_0 t + \theta)) \\
& + f_6 A^2 \sin(2(\omega_0 t + \theta)) + (t - t_0) f_7 A^2 \cos(2(\omega_0 t + \theta)) + (t - t_0) f_8 A^2 \sin(2(\omega_0 t + \theta)) \\
& + f_9 A^3 \cos(3(\omega_0 t + \theta)) + f_{10} A^3 \sin(3(\omega_0 t + \theta)) + f_{11} A^2 + (t - t_0) f_{12} A^2, \tag{31}
\end{aligned}$$

where  $f_{1a}$ ,  $f_{1b}$ ,  $f_{2a}$ ,  $f_{2b}$ , and  $f_k$  ( $k = 3 \cdots 12$ ) are constants depending on Eqs. (26), (28), and (30). Note that the solution is constructed so that the secular terms vanish at  $t = t_0$ .

Thus, collecting all of the terms, the approximate solution to Eq. (22) up to the third order of  $\varepsilon$  reads

$$\begin{aligned}
x(t; t_0) = & x_0 + \varepsilon A \cos(\omega_0 t + \theta) + \varepsilon^2 \{ (t - t_0) d_1 A \cos(\omega_0 t + \theta) + (t - t_0) d_2 A \sin(\omega_0 t + \theta) \\
& + d_3 A^2 \cos(2(\omega_0 t + \theta)) + d_4 A^2 \sin(2(\omega_0 t + \theta)) + d_5 A^2 \} \\
& + \varepsilon^3 \{ (t - t_0)(f_{1a}A^3 + f_{1b}A) \cos(\omega_0 t + \theta) + (t - t_0)(f_{2a}A^3 + f_{2b}A) \sin(\omega_0 t + \theta) \\
& + (t - t_0)^2 f_3 A \cos(\omega_0 t + \theta) + (t - t_0)^2 f_4 A \sin(\omega_0 t + \theta) + f_5 A^2 \cos(2(\omega_0 t + \theta)) \\
& + f_6 A^2 \sin(2(\omega_0 t + \theta)) + (t - t_0) f_7 A^2 \cos(2(\omega_0 t + \theta)) + (t - t_0) f_8 A^2 \sin(2(\omega_0 t + \theta)) \\
& + f_9 A^3 \cos(3(\omega_0 t + \theta)) + f_{10} A^3 \sin(3(\omega_0 t + \theta)) + f_{11} A^2 + (t - t_0) f_{12} A^2 \} + o(\varepsilon^3). \tag{32}
\end{aligned}$$

Because Eq. (32) contains the secular terms, this solution is valid only locally around  $t = t_0$ , but it exhibits a divergent behavior as  $|t - t_0|$  goes infinity. In fact, this is a rather common behavior occurring in naïve perturbation expansions.

Next, we use a geometrical viewpoint to circumvent the disastrous situation following [41]. The solution (32) gives a family of curves with  $t_0$  being the parameter specifying each curve in the  $t$ - $x$  plane. Each curve gives a good approximate solution to the original equation in a local domain around  $t = t_0$ . The idea is that the envelope curve of the family of curves hopefully gives an approximate but valid solution in the global domain including the arbitrary time  $t_0$ . Indeed, this has rigorously been demonstrated to be the case [41, 43, 53]. Now, the envelope

curve can be constructed using the following envelope equation [41]:

$$\left. \frac{dx(t; t_0)}{dt_0} \right|_{t_0=t} = \left. \frac{\partial x}{\partial t_0} \right|_{t_0=t} + \left. \frac{dA(t_0)}{dt_0} \frac{\partial x}{\partial A} \right|_{t_0=t} + \left. \frac{d\theta(t_0)}{dt_0} \frac{\partial x}{\partial \theta} \right|_{t_0=t} = 0. \quad (33)$$

Note that we have taken into account the fact that the integral constants  $A$  and  $\theta$  depend on the ‘initial time’  $t = t_0$ , and (33) actually gives the dynamical equations for these variables. As will be done shortly, the insertion of the solutions to the dynamic equation into (32) gives an approximate but globally valid solution to the original equation. Because the envelope equation (33) takes a similar form as the RG equation in quantum field theory, it is also called the RG equation, and the asymptotic/global analysis based on this equation was named the RG method [39].

Substituting Eq. (32) into Eq. (33), we have

$$\begin{aligned} 0 = & \varepsilon \left\{ \frac{dA}{dt} - \varepsilon^2 f_{1a} A^3 - \varepsilon(d_1 + \varepsilon f_{1b})A \right\} \cos(\omega_0 t + \theta) \\ & + \varepsilon A \left\{ -\frac{d\theta}{dt} - \varepsilon^2 f_{2a} A^2 - \varepsilon(d_2 + \varepsilon f_{2b}) \right\} \sin(\omega_0 t + \theta) \\ & + \varepsilon^2 A \left\{ 2(d_3 + \varepsilon f_5) \frac{dA}{dt} + 2(d_4 + \varepsilon f_6) A \frac{d\theta}{dt} - \varepsilon f_7 A \right\} \cos(2(\omega_0 t + \theta)) \\ & + \varepsilon^2 A \left\{ 2(d_4 + \varepsilon f_6) \frac{dA}{dt} - 2(d_3 + \varepsilon f_5) A \frac{d\theta}{dt} - \varepsilon f_8 A \right\} \sin(2(\omega_0 t + \theta)) \\ & + 3\varepsilon^3 A^2 \left\{ f_9 \frac{dA}{dt} + f_{10} A \frac{d\theta}{dt} \right\} \cos(3(\omega_0 t + \theta)) + 3\varepsilon^3 A^2 \left\{ f_{10} \frac{dA}{dt} - f_9 A \frac{d\theta}{dt} \right\} \sin(3(\omega_0 t + \theta)) \\ & + 2\varepsilon^2 (d_5 + \varepsilon f_{11}) A \frac{dA}{dt} - \varepsilon^3 f_{12} A + o(\varepsilon^3). \end{aligned} \quad (34)$$

Because  $dA/dt$  and  $d\theta/dt$  are of order  $\varepsilon$ , the coefficients  $\cos(2(\omega_0 t + \theta))$ ,  $\sin(2(\omega_0 t + \theta))$ ,  $\cos(3(\omega_0 t + \theta))$ ,  $\sin(3(\omega_0 t + \theta))$ , and  $A dA/dt$  are of order  $\varepsilon^3$  or higher. To make Eq. (34) hold for any  $t$ , we only must ensure that the coefficients of the independent functions, namely  $\cos(\omega_0 t + \theta)$  and  $\sin(\omega_0 t + \theta)$ , vanish, and hence, we have

$$\frac{dA}{dt} = \varepsilon^2 f_{1a} A^3 + \varepsilon(d_1 + \varepsilon f_{1b})A + o(\varepsilon^2), \quad (35)$$

$$\frac{d\theta}{dt} = -\varepsilon^2 f_{2a} A^2 - \varepsilon(d_2 + \varepsilon f_{2b}) + o(\varepsilon^2), \quad (36)$$

which are the dynamic equations governing the 'integral constants'  $A$  and  $\theta$ . We now see that the integral constants have been lifted to dynamic variables through the RG/envelope equation. The amplitude equation (35) can be readily solved analytically. For instance, when  $f_{1a} < 0$  and  $d_1 + \varepsilon f_{1b} > 0$ , it yields

$$A(t) = A_0 \frac{\mathcal{A}}{\sqrt{\mathcal{A}^2 + (A_0^2 - \mathcal{A}^2)e^{-2\alpha t}}}, \quad (37)$$

where  $\alpha = \varepsilon(d_1 + \varepsilon f_{1b})$  and

$$A_0 = \sqrt{-\frac{d_1 + \varepsilon f_{1b}}{\varepsilon f_{1a}}}, \quad (38)$$

with  $\mathcal{A}$  being the initial amplitude. Equation (37) indicates that the amplitude approaches  $A_0$  monotonically as  $t \rightarrow \infty$ , implying that  $A_0$  is nothing but the amplitude of the limit cycle admitted in the original equation (22). Furthermore, Eq. (36) indicates that the angular frequency on the limit cycle reads

$$\omega = \omega_0 + (d\theta/dt)|_{A=A_0} = \omega_0 - \varepsilon \frac{d_2 f_{1a} - d_1 f_{2a}}{f_{1a}}, \quad (39)$$

which is constant. The globally valid solution is given as the envelope of the family of curves, as previously stated. Thus, the solution on the limit cycle, which valid in a global domain in the asymptotic regime, reads

$$\begin{aligned} x(t) &= x(t; t_0)|_{t_0=t} \\ &= x_0 + \varepsilon A_0 \cos(\omega t + \theta_0) + \varepsilon^2 \{d_3 A_0^2 \cos(2(\omega t + \theta_0)) + d_4 A_0^2 \sin(2(\omega t + \theta_0)) + d_5 A_0^2\} \\ &\quad + \varepsilon^3 \{f_5 A_0^2 \cos(2(\omega t + \theta_0)) + f_6 A_0^2 \sin(2(\omega t + \theta_0)) + f_9 A_0^3 \cos(3(\omega t + \theta_0)) \\ &\quad + f_{10} A_0^3 \sin(3(\omega t + \theta_0)) + f_{11} A_0^2\} + o(\varepsilon^3). \end{aligned} \quad (40)$$

The RG method is a powerful method for obtaining a globally valid solution. This method can be applied to various models including discrete, stochastic, and partial differential equations, as given in [54, 60].



## A.2 Derivation of a time-evolution solution in a circadian rhythm model using the RG method

In this subsection, we applied the RG method to derive an approximate but globally valid solution of the circadian clock model given by Eq. (2)-(4), which is a system of first-order equations with three variables. We first convert the system into a single equation with higher-order derivatives as

$$\frac{d^3 x_3}{dt^3} + s_1 \frac{d^2 x_3}{dt^2} + s_2 \frac{dx_3}{dt} + s_3 x_3 = p_1 p_2 f(x_3) \quad (41)$$

where  $s_1 = k_1 + k_2 + k_3$ ,  $s_2 = k_1 k_2 + k_2 k_3 + k_3 k_1$ ,  $s_3 = k_1 k_2 k_3$ . To obtain the approximate solution, we set the transcriptional regulator  $f(x_3)$  as  $r/x_3^n$ . This model has a fixed point

$$x_0 = \left( \frac{s_3}{p_1 p_2 r} \right)^{-\frac{1}{n+1}}, \quad (42)$$

which is destabilized through Hopf bifurcation for

$$n > n_0 \equiv \frac{s_4}{s_3}, \quad (43)$$

with  $s_4 = (k_1 + k_2)(k_2 + k_3)(k_3 + k_1)$ .

Then, we expand the solution around  $t = t_0$  as a series of  $\varepsilon$

$$x_3(t; t_0) = x_0 + \varepsilon u_1(t; t_0) + \varepsilon^2 u_2(t; t_0) + \varepsilon^3 u_3(t; t_0) + O(\varepsilon^3). \quad (44)$$

Substituting Eq. (44) into Eq. (41) and equating the coefficients with the same powers of  $\varepsilon$ , we obtain

$$O(\varepsilon) : \frac{d^3 u_1}{dt^3} + s_1 \frac{d^2 u_1}{dt^2} + s_2 \frac{du_1}{dt} + s_1 s_2 u_1 = 0, \quad (45)$$

$$O(\varepsilon^2) : \frac{d^3 u_2}{dt^3} + s_1 \frac{d^2 u_2}{dt^2} + s_2 \frac{du_2}{dt} + s_1 s_2 u_2 = -s_3 u_1 + B_1 u_1^2, \quad (46)$$

$$O(\varepsilon^3) : \frac{d^3 u_3}{dt^3} + s_1 \frac{d^2 u_3}{dt^2} + s_2 \frac{du_3}{dt} + s_1 s_2 u_3 = -s_3 u_2 + B_2 u_1 u_2 + B_3 u_1^2 + B_4 u_1^3, \quad (47)$$

where

$$B_1 = \frac{s_4 s_2 s_1}{2s_3} \left( \frac{s_3}{p_1 p_2 r} \right)^{\frac{s_3}{s_1 s_2}}, \quad (48)$$

$$B_2 = \frac{s_4 s_2 s_1}{s_3} \left( \frac{s_3}{p_1 p_2 r} \right)^{\frac{s_3}{s_1 s_2}}, \quad (49)$$

$$B_3 = \left\{ s_4 + \frac{s_3}{2} - \left( \frac{s_4 s_3}{2s_2 s_1} \ln \left( \frac{s_3}{p_1 p_2 r} \right) \right) \right\} \left( \frac{s_3}{p_1 p_2 r} \right)^{\frac{s_3}{s_1 s_2}}, \quad (50)$$

$$B_4 = \frac{(s_2 s_1 + s_3) s_4 s_1 s_2}{6s_3^2} \left( \frac{2s_3}{p_1 p_2 r} \right)^{\frac{s_3}{s_1 s_2}}. \quad (51)$$

Because Eq. (45) has three eigenvalues, namely  $\lambda_{1,2} = \pm i\sqrt{s_2}$  and  $\lambda_3 = -s_1$ , the general solution of Eq. (45) reads

$$u_1(t; t_0) = A(t_0) \cos(\omega_0 t + \theta(t_0)) + c(t_0) e^{-s_1 t}, \quad (\omega_0 := \sqrt{s_2}), \quad (52)$$

where  $A$ ,  $\theta$ , and  $c$  are integral constants that depend on initial time  $t_0$ .

Considering the asymptotic regime in which the second term in Eq. (52) is so small and negligible, then the first-order solution can be written as

$$u_1(t; t_0) = A(t_0) \cos(\omega_0 t + \theta(t_0)). \quad (53)$$

Substituting Eq. (53) into Eq. (46), we obtain

$$\frac{d^3 u_2}{dt^3} + s_1 \frac{d^2 u_2}{dt^2} + s_2 \frac{du_2}{dt} + s_1 s_2 u_2 = -s_3 A \cos(\omega_0 t + \theta) + C A^2 \cos(2\omega_0 t + 2\theta) + C A^2, \quad (54)$$

where

$$C = \frac{s_4 s_1 s_2}{4s_3} \left( \frac{s_3}{p_1 p_2 r} \right)^{\frac{s_3}{s_1 s_2}}. \quad (55)$$

Equation (54) is an inhomogeneous equation that contains a zero mode of the linear operator,

and the solution having a suitable form for applying the RG method is written as

$$u_2(t; t_0) = D_1 A(t - t_0) \cos(\omega_0 t + \theta) - D_2 A(t - t_0) \sin(\omega_0 t + \theta) \\ - D_3 A^2 \cos(2\omega_0 t + 2\theta) - D_4 A^2 \sin(2\omega_0 t + 2\theta) + D_5 A^2, \quad (56)$$

where the coefficients are

$$D_1 = \frac{s_3}{2(s_1^2 + s_2)}, \quad (57)$$

$$D_2 = \frac{s_1 s_3}{2\sqrt{s_2}(s_1^2 + s_2)}, \quad (58)$$

$$D_3 = \frac{s_4 s_1^2}{12(s_1^2 + 4s_2)s_3} \left( \frac{s_3}{p_1 p_2 r} \right)^{\frac{s_3}{s_1 s_2}}, \quad (59)$$

$$D_4 = \frac{s_4 s_1 \sqrt{s_2}}{6(s_1^2 + 4s_2)s_3} \left( \frac{s_3}{p_1 p_2 r} \right)^{\frac{s_3}{s_1 s_2}}, \quad (60)$$

$$D_5 = \frac{s_4}{4s_3} \left( \frac{s_3}{p_1 p_2 r} \right)^{\frac{s_3}{s_1 s_2}}. \quad (61)$$

Tentatively, after collecting all the obtained terms, we have the approximate solution in the second order as

$$x_3(t; t_0) = x_0 + \varepsilon A \cos(\omega_0 t + \theta) + \varepsilon^2 \{ D_1 A(t - t_0) \cos(\omega_0 t + \theta) - D_2 A(t - t_0) \sin(\omega_0 t + \theta) \\ - D_3 A^2 \cos(2\omega_0 t + 2\theta) - D_4 A^2 \sin(2\omega_0 t + 2\theta) + D_5 A^2 \} + o(\varepsilon^2). \quad (62)$$

Because it contains the secular terms, the solution diverges as  $|t - t_0|$  goes infinity. To resum the would-be divergent terms, we apply the RG equation  $dx_3(t, t_0)/dt|_{t_0=t}$ , which leads to the equations governing the amplitude and phase as

$$dA/dt = \varepsilon s_3 A / 2(s_1^2 + s_2),$$

and

$$d\theta/dt = \varepsilon s_1 s_3 / 2\sqrt{s_2}(s_1^2 + s_2),$$

nicely describing the slow motions of the amplitude and phase, respectively. However, it fails to describe a transitional behavior approaching a limit cycle, as indicated by the present model.

Therefore, we analyzed the third-order equation, which might lead to a limit cycle solution. Substituting Eqs. (53) and (56) into Eq. (47), we have

$$\begin{aligned}
\frac{d^3u_3}{dt^3} + s_1 \frac{d^2u_3}{dt^2} + s_2 \frac{du_3}{dt} + s_1s_2u_3 &= E_1A^3 \cos(\omega_0t + \theta) - E_2A^3 \sin(\omega_0t + \theta) \\
&- E_3A(t - t_0) \cos(\omega_0t + \theta) + E_4A(t - t_0) \sin(\omega_0t + \theta) + E_5A^2 \cos(2\omega_0t + 2\theta) \\
&+ E_6A^2 \sin(2\omega_0t + 2\theta) + E_7A^2(t - t_0) \cos(2\omega_0t + 2\theta) - E_8A^2(t - t_0) \sin(2\omega_0t + 2\theta) \\
&- E_9A^3 \cos(3\omega_0t + 3\theta) - E_{10}A^3 \sin(3\omega_0t + 3\theta) + E_{11}A^2 + E_{12}A^2(t - t_0). \tag{63}
\end{aligned}$$

where

$$E_1 = \frac{(s_1^2 s_2 - 4s_1^2 s_3 + 6s_1 s_2^2 - 18s_2 s_3) s_4 s_1 s_2}{12(s_1^2 + 4s_2) s_3^2} \left( \frac{s_3}{p_1 p_2 r} \right)^{\frac{2s_3}{s_1 s_2}}, \quad (64)$$

$$E_2 = \frac{s_4^2 s_1^2 \sqrt{s_2^3}}{12(s_1^2 + 4s_2) s_3^2} \left( \frac{s_3}{p_1 p_2 r} \right)^{\frac{2s_3}{s_1 s_2}}, \quad (65)$$

$$E_3 = \frac{s_3^2}{2(s_1^2 + s_2)}, \quad (66)$$

$$E_4 = \frac{s_1 s_3^2}{2(s_1^2 + s_2) \sqrt{s_2}}, \quad (67)$$

$$E_5 = \left\{ \frac{7s_1^3 s_2 - 4s_1^2 s_3 + 24s_1 s_2^2 - 12s_2 s_3}{12(s_1^2 + 4s_2)} - \frac{s_4 s_3}{4s_1 s_2} \ln \left( \frac{s_3}{p_1 p_2 r} \right) \right\} \left( \frac{s_3}{p_1 p_2 r} \right)^{\frac{s_3}{s_1 s_2}}, \quad (68)$$

$$E_6 = \frac{s_4 s_1 \sqrt{s_2}}{6(s_1^2 + 4s_2)} \left( \frac{s_3}{p_1 p_2 r} \right)^{\frac{s_3}{s_1 s_2}}, \quad (69)$$

$$E_7 = \frac{s_4 s_1 s_2}{4(s_1^2 + s_2)} \left( \frac{s_3}{p_1 p_2 r} \right)^{\frac{s_3}{s_1 s_2}}, \quad (70)$$

$$E_8 = \frac{s_4 s_1^2 \sqrt{s_2}}{4(s_1^2 + s_2)} \left( \frac{s_3}{p_1 p_2 r} \right)^{\frac{s_3}{s_1 s_2}}, \quad (71)$$

$$E_9 = \frac{((s_1^2 + 2s_2) s_1 + 2s_3) s_4 s_1 s_2^2}{12(s_1^2 + 4s_2) s_3^2} \left( \frac{s_3}{p_1 p_2 r} \right)^{\frac{2s_3}{s_1 s_2}}, \quad (72)$$

$$E_{10} = \frac{s_4^2 s_1^2 \sqrt{s_2^3}}{12(s_1^2 + 4s_2) s_3^2} \left( \frac{s_3}{p_1 p_2 r} \right)^{\frac{2s_3}{s_1 s_2}}, \quad (73)$$

$$E_{11} = \frac{1}{4} \left\{ s_1 s_2 - \frac{s_4 s_3}{s_1 s_2} \ln \left( \frac{s_3}{p_1 p_2 r} \right) \right\} \left( \frac{s_3}{p_1 p_2 r} \right)^{\frac{2s_3}{s_1 s_2}}, \quad (74)$$

$$E_{12} = \frac{s_4 s_1 s_2}{4(s_1^2 + s_2)} \left( \frac{s_3}{p_1 p_2 r} \right)^{\frac{s_3}{s_1 s_2}}. \quad (75)$$

The solution to Eq. (63) is given by

$$\begin{aligned} u_3(t; t_0) = & - (F_{1a} A^3 + F_{1b} A)(t - t_0) \cos(\omega_0 t + \theta) + (F_{2a} A^3 + F_{2b} A)(t - t_0) \sin(\omega_0 t + \theta) \\ & - F_3 A(t - t_0)^2 \cos(\omega_0 t + \theta) - F_4 A(t - t_0)^2 \sin(\omega_0 t + \theta) + F_5 A^2 \cos(2\omega_0 t + 2\theta) \\ & + F_6 A^2 \sin(2\omega_0 t + 2\theta) - F_7 A^2(t - t_0) \cos(2\omega_0 t + 2\theta) \\ & + F_8 A^2(t - t_0) \sin(2\omega_0 t + 2\theta) + F_9 A^3 \cos(3\omega_0 t + 3\theta) + F_{10} A^3 \sin(3\omega_0 t + 3\theta) \\ & + F_{11} A^2 + F_{12} A^2(t - t_0) \end{aligned} \quad (76)$$

where

$$F_{1a} = \frac{(2s_1s_2^2 - (s_1^2 + 6s_2)s_3)s_4s_1s_2}{8(s_1^2 + 4s_2)(s_1^2 + s_2)s_3^2} \left( \frac{s_3}{p_1p_2r} \right)^{\frac{2s_3}{s_1s_2}}, \quad (77)$$

$$F_{1b} = \frac{s_1s_3^2}{(s_1^2 + s_2)^3}, \quad (78)$$

$$F_{2a} = \frac{((s_1^2 + 7s_2)s_1s_2 - (4s_1^2 + 19s_2)s_3)s_4s_1^2\sqrt{s_2}}{24(s_1^2 + s_2)(s_1^2 + 4s_2)s_3^2} \left( \frac{s_3}{p_1p_2r} \right)^{\frac{2s_3}{s_1s_2}}, \quad (79)$$

$$F_{2b} = \frac{((s_1^2 + 6s_2)s_1^2 - 3s_2^2)s_3^2}{8(s_1^2 + s_2)^3\sqrt{s_2^3}}, \quad (80)$$

$$F_3 = \frac{(s_1^2 - s_2)s_3^2}{8(s_1^2 + s_2)s_2}, \quad (81)$$

$$F_4 = \frac{s_1s_3^2}{4(s_1^2 + s_2)\sqrt{s_2}}, \quad (82)$$

$$F_5 = \left\{ \frac{s_4s_3}{12(s_1^2 + 4s_2)s_2^2} \ln \left( \frac{s_3}{p_1p_2r} \right) - \frac{(3s_1^5 + 4s_1^3s_2 + 11s_1^2s_3 + 64s_1s_2^2 - 52s_2s_3)s_1}{36(s_1^2 + s_2)(s_1^2 + 4s_2)^2} \right\} \left( \frac{s_3}{p_1p_2r} \right)^{\frac{s_3}{s_1s_2}}, \quad (83)$$

$$F_6 = \left\{ \frac{s_4s_3}{6(s_1^2 + 4s_2)s_1\sqrt{s_2^3}} \ln \left( \frac{s_3}{p_1p_2r} \right) - \frac{7s_1^5s_2 - s_1^4s_3 - 8s_1^3s_2^2 + 38s_1^2s_2s_3 + 48s_1s_2^3 - 24s_2^2s_3}{36(s_1^2 + s_2)(s_1^2 + 4s_2)^2\sqrt{s_2}} \right\} \left( \frac{s_3}{p_1p_2r} \right)^{\frac{s_3}{s_1s_2}}, \quad (84)$$

$$F_7 = \frac{s_4s_1^2}{4(s_1^2 + s_2)(s_1^2 + 4s_2)} \left( \frac{s_3}{p_1p_2r} \right)^{\frac{s_3}{s_1s_2}}, \quad (85)$$

$$F_8 = \frac{(s_1^2 - 2s_2)s_4s_1}{12(s_1^2 + s_2)(s_1^2 + 4s_2)\sqrt{s_2}} \left( \frac{s_3}{p_1p_2r} \right)^{\frac{s_3}{s_1s_2}}, \quad (86)$$

$$F_9 = \frac{(s_1(s_1^2 - s_2) + 5s_3)s_4s_1^2s_2}{96(s_1^2 + 4s_2)(s_1^2 + 9s_2)s_3^2} \left( \frac{s_3}{p_1p_2r} \right)^{\frac{2s_3}{s_1s_2}}, \quad (87)$$

$$F_{10} = \frac{(2(2s_1^2 + 3s_2)s_1s_2 + (6s_2 - s_1^2)s_3)s_4s_1\sqrt{s_2}}{96(s_1^2 + 4s_2)(s_1^2 + 9s_2)s_3^2} \left( \frac{s_3}{p_1p_2r} \right)^{\frac{2s_3}{s_1s_2}}, \quad (88)$$

$$F_{11} = \left\{ \frac{(s_1^3 + s_3)}{4(s_1^2 + s_2)s_1} - \frac{s_4s_3}{4s_1^2s_2^2} \ln \left( \frac{s_3}{p_1p_2r} \right) \right\} \left( \frac{s_3}{p_1p_2r} \right)^{\frac{s_3}{s_1s_2}}, \quad (89)$$

$$F_{12} = \frac{s_4}{4(s_1^2 + s_2)} \left( \frac{s_3}{p_1p_2r} \right)^{\frac{s_3}{s_1s_2}}. \quad (90)$$

To obtain a globally valid solution using Eq. (76), we apply the RG method, which utilizes the

RG equation

$$\begin{aligned}
\left. \frac{dx_3(t; t_0)}{dt_0} \right|_{t_0=t} &= \left. \frac{\partial x_3(t; t_0)}{\partial t_0} \right|_{t_0=t} + \left. \frac{dA}{dt_0} \frac{\partial x_3(t; t_0)}{\partial A} \right|_{t_0=t} + \left. \frac{d\theta}{dt_0} \frac{\partial x_3(t; t_0)}{\partial \theta} \right|_{t_0=t} \\
&= \left\{ \varepsilon \frac{dA}{dt} - \varepsilon D_1 A + \varepsilon^3 (F_{1a} A^3 + F_{1b} A) \right\} \cos(\omega_0 t + \theta) \\
&\quad + \left\{ -\varepsilon A \frac{d\theta}{dt} + \varepsilon^2 D_2 A - \varepsilon^3 (F_{2a} A^3 + F_{2b} A) \right\} \sin(\omega_0 t + \theta) = 0, \quad (91)
\end{aligned}$$

where we have neglected the higher-order terms  $o(\varepsilon^3)$ . For Eq. (91) to hold for any  $t$ , the coefficients of the two independent functions should vanish. Thus, we obtain the dynamic equations for  $A$  and  $\theta$ :

$$\frac{dA}{dt} = \varepsilon D_1 A - \varepsilon^2 (F_{1a} A^3 + F_{1b} A) + o(\varepsilon^2), \quad (92)$$

$$\frac{d\theta}{dt} = \varepsilon D_2 - \varepsilon^2 (F_{2a} A^2 + F_{2b}) + o(\varepsilon^2). \quad (93)$$

The amplitude equation (92) has a new fixed point

$$A_0 = \sqrt{\frac{D_1 - \varepsilon F_{1b}}{\varepsilon F_{1a}}} = \sqrt{\frac{4((s_1^2 + s_2)^2 - 2\varepsilon s_1 s_3)(s_1^2 + 4s_2)s_3^3}{\varepsilon(2s_1 s_2^2 - (s_1^2 + 6s_2)s_3)(s_1^2 + s_2)^2 s_4 s_1 s_2} \left( \frac{p_1 p_2 r}{s_3} \right)^{\frac{s_3}{s_1 s_2}}}, \quad (94)$$

which is nothing but the amplitude of the desired limit cycle. The phase function  $\theta(t)$  on the limit cycle is expressed as

$$\theta(t) = (\varepsilon D_2 - \varepsilon^2 (F_{2a} A_0^2 + F_{2b}) + o(\varepsilon^2))t + \theta_0, \quad (95)$$

where  $\theta_0$  is the integral constant and it gives the initial phase at  $t = 0$ . Substituting Eqs. (58), (79), (80) and (94) into (95),  $\theta(t)$  is reduced to

$$\theta(t) = \left\{ -\varepsilon \frac{s_1 s_3 s_4}{6(2s_1 s_2^2 - (s_1^2 + 6s_2)s_3)\sqrt{s_2}} + o(\varepsilon) \right\} t + \theta_0. \quad (96)$$

Thus, the solution describing the limit cycle, which is valid in a global domain in the asymptotic

regime, is given by

$$\begin{aligned}
x_3(t) &= x_3(t; t_0)|_{t_0=t} \\
&= x_0 + \varepsilon A_0 \cos(\omega t + \theta_0) \\
&\quad - \varepsilon^2 \{D_3 A_0^2 \cos(2(\omega t + \theta_0)) + D_4 A_0^2 \sin(2(\omega t + \theta_0))\} + o(\varepsilon^2).
\end{aligned} \tag{97}$$

In particular, if the initial phase is set to be  $\theta_0 = -\pi/2$ , we have Eq. (7).

### A.3 Numerical and RG analyses of the Lotka-Volterra model

Equation (5) and the numerical simulation indicate that non-sinusoidal power ( $NS$ ) tends to be larger when the period hardly changes and is stable in response to increases of the parameter values specifying the degradation rates, as presented in Fig. 1B. This suggests that the waveform becomes more distorted at higher temperatures when the circadian period is temperature-compensated. It was previously reported that the same conclusion holds for other oscillatory models, including a realistic mammalian circadian clock model, a post-translational model in cyanobacteria, and the van der Pol oscillator [31, 63]. However, it is important to note that the findings using specific mathematical models might not be universally applicable to other models and actual organisms. Therefore, one should examine whether the waveform also plays a crucial role in the stability of the period in other oscillatory models.

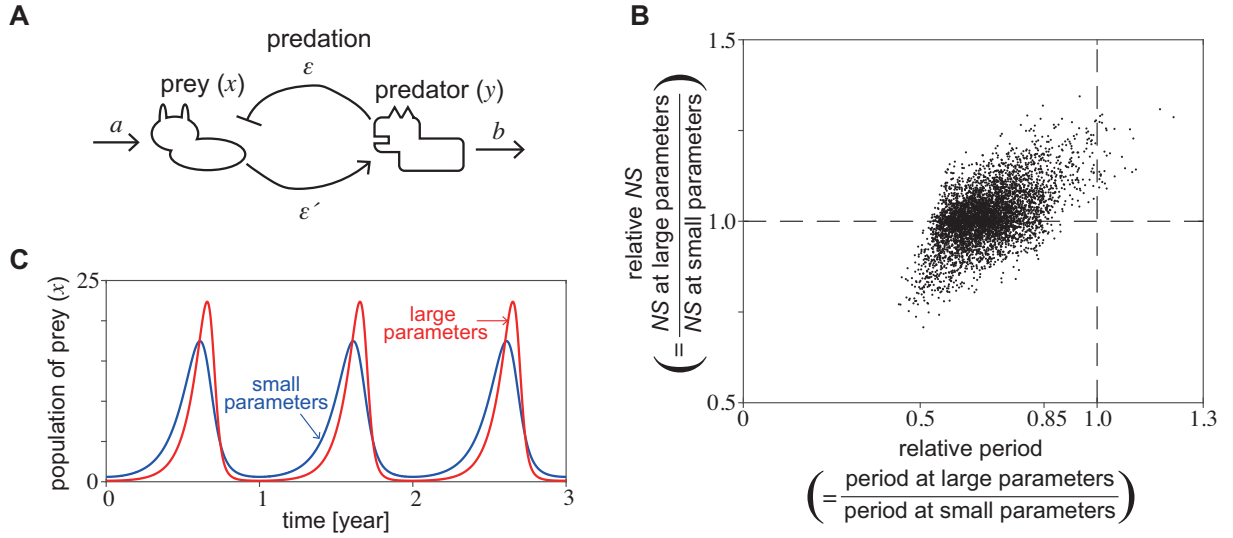
Thus, we conduct a numerical simulation to test the possible period-waveform correlation in the Lotka-Volterra model as done for the circadian clock model. Needless to say, the Lotka-Volterra model is one of the most extensively studied mathematical models in biology [65], and it effectively explains population dynamics in prey-predator systems. The Lotka-Volterra model is given as a system with two variables as

$$\frac{dx}{dt} = ax - \varepsilon xy, \tag{98}$$

$$\frac{dy}{dt} = -by + \varepsilon' xy, \tag{99}$$

where  $x(t)$  and  $y(t)$  are numbers of prey and predators. Parameter  $a$  is the growth rate of prey,  $b$  is the death rate of predators,  $\varepsilon$  is the death rate of prey attributable to predation, and  $\varepsilon'$  is the growth rate of predators (Supplementary Fig. 1A).





Supplementary Figure 1: (A) Lotka-Volterra model. (B) Distribution of relative  $NS$  for  $x(t)$  of the Lotka-Volterra model as a function of the relative period when rate constants are increased. We first generated reference parameter sets. Then, each parameter  $a$ ,  $b$ ,  $\varepsilon$ , and  $\varepsilon'$  in the model's reference parameter set was randomly multiplied by a factor of 1.1-1.9. (C) Examples of the waveform in the Lotka-Volterra model when the period is relatively unchanged. The blue and red lines represent small and large parameters, respectively.

In the present numerical simulation, we first generated 100 reference parameter sets corresponding to the reference temperature. The values of the model parameters  $a$  and  $b$  were generated randomly with a uniform distribution between 0 and 1, and similarly, the values of the other model parameters  $\varepsilon$  and  $\varepsilon'$  were also randomly assigned values between 0 and 0.5. The period obtained for each parameter set with the initial condition  $(x_0, y_0) = (2, 2)$  was denoted as  $\tau_1$ . Next,  $a$ ,  $b$ ,  $\varepsilon$ , and  $\varepsilon'$  were multiplied by a random factor within the range of 1.1-1.9 to simulate the increase in temperature, yielding 49 oscillatory parameter sets. Each resulting new period was denoted as  $\tau_2$ , and thus, the ratio of the period  $= \tau_2/\tau_1$ , which is called the relative period, was obtained.

The numerical simulations reveal a consistent positive correlation between  $NS$  and the relative period (Supplementary Fig. 1BC). A notable point is that the value of  $NS$  tends to increase along with the period when larger multiplicative factors are used in the simulation. This result again suggests that our findings that the waveform becomes more distorted when the period remains relatively stable in response to increased parameter values is a rather universal phe-

nomenon not restricted to the behavior observed in the circadian clock model (Fig. 2A).

The period of the Lotka-Volterra model, together with its approximate but globally valid solution, was previously derived analytically by one of the present authors [43, 53] on the basis of the RG method; see also the pioneering work [68] based on a different method. Next, we will demonstrate that the expression explicitly reveals that the period of the Lotka-Volterra model almost linearly increases with the waveform distortion for the average of the prey-predator time series (i.e.  $\overline{NS}$ ). In the mathematical analysis, it proved convenient to use new variables  $(\xi(t), \eta(t))$  defined as

$$x(t) = (b + \varepsilon\xi(t))/\varepsilon', \quad y(t) = a/\varepsilon + \eta(t).$$

The RG method performed in [44, 53] in the second order of  $\varepsilon$  leads to

$$\begin{aligned} \xi(t) = & \left(1 - \varepsilon^2 \frac{a-b}{4ab^2} \frac{A^2}{12}\right) A \sin \Theta - \varepsilon^2 \frac{1}{b\sqrt{ab}} \frac{A^2}{24} \cos \Theta - \varepsilon \frac{1}{\sqrt{ab}} \frac{A^2}{6} \sin(2\Theta) \\ & - \varepsilon \frac{1}{b} \frac{A^2}{3} \cos(2\Theta) - \varepsilon^2 \frac{3a-b}{4ab^2} \frac{A^3}{8} \sin(3\Theta) + \varepsilon^2 \frac{1}{b\sqrt{ab}} \frac{A^2}{8} \cos(3\Theta) + o(\varepsilon^2), \end{aligned} \quad (100)$$

$$\begin{aligned} \eta(t) = & \varepsilon^2 \frac{1}{b^2} \frac{A^3}{24} \sin \Theta - \frac{\sqrt{ab}}{b} \left(1 + \varepsilon^2 \frac{a-b}{4ab^2} \frac{A^2}{12}\right) A \cos \Theta - \varepsilon \frac{\sqrt{ab}}{b^2} \frac{A^2}{6} \sin(2\Theta) \\ & + \varepsilon \frac{1}{b} \frac{A^2}{3} \cos(2\Theta) + \varepsilon^2 \frac{1}{b^2} \frac{A^3}{8} \sin(3\Theta) + \varepsilon^2 \frac{a-3b}{4b^2\sqrt{ab}} \frac{A^3}{8} \cos(3\Theta) + o(\varepsilon^2), \end{aligned} \quad (101)$$

where  $A$  and  $\theta$  are the integral constants, which are to be determined by the initial condition, and  $\Theta = \tilde{\omega}t + \theta$ , with  $\tilde{\omega}$  being the angular frequency given by

$$\tilde{\omega} = \sqrt{ab} \left\{ 1 - \frac{\varepsilon^2 A^2 (a+b)}{24ab^2} \right\}, \quad (102)$$

from which we have the formula of the period of the system after some manipulation as

$$\tau = \frac{2\pi}{\tilde{\omega}} = \frac{2\pi}{\sqrt{ab}} \left\{ \frac{2}{5} \left( 1 + \frac{5\varepsilon^2 A^2 (a+b)}{24ab^2} \right) + \frac{3}{5} \right\} + o(\varepsilon^2). \quad (103)$$

From the waveforms for  $\xi(t)$  and  $\eta(t)$  given by (100) and (101), respectively, we can obtain the waveform distortion of each variable as follows:

$$NS(\xi) = 1 + \frac{\varepsilon^2 A^2 (4a+b)}{24ab^2} + o(\varepsilon^2), \quad (104)$$

$$NS(\eta) = 1 + \frac{\varepsilon^2 A^2 (a+4b)}{24ab^2} + o(\varepsilon^2). \quad (105)$$

It is notable that the mean of  $NS^{(\xi)}$  and  $NS^{(\eta)}$  takes the form

$$\overline{NS} = \frac{1}{2}(NS^{(\xi)} + NS^{(\eta)}) = 1 + \frac{5}{2} \frac{\varepsilon^2 A^2 (a+b)}{24ab^2} + o(\varepsilon^2). \quad (106)$$

Indeed, comparing (106) and (103), we arrive at

$$\tau = \frac{2\pi}{\sqrt{ab}} \left( \frac{2}{5} \overline{NS} + \frac{3}{5} \right) + o(\varepsilon^2), \quad (107)$$

which states that the period and the mean waveform distortion, namely  $\overline{NS}$ , are linearly dependent on each other, and they tend to increase (or decrease) in a parallel manner. This is what we aimed to demonstrate for the Lotka-Volterra model.

#### A.4 Numerical and RG analyses of the van der Pol model

We consider the van der Pol model as follows:

$$\frac{d^2 x}{dt^2} + x = \varepsilon(1 - x^2) \frac{dx}{dt}, \quad (108)$$

which is known as one of the fundamental non-linear oscillator models. Previously, two of the authors derived the period formula  $\tau = 2\pi[\sum_{j=1}^{\infty} |a_j|^2 j^2 / \sum_{j=1}^{\infty} |a_j|^2]^{1/2}$ , meaning that the period of the model is also proportional to  $NS$  [31]. Then, we derive the approximate solution of the model using the RG method and confirm the proportionality between the period and the waveform distortion  $NS$  in detail. First, we represent the local solution around  $t = t_0$  as a perturbation series

$$x(t; t_0) = x_0(t; t_0) + \varepsilon x_1(t; t_0) + \varepsilon^2 x_2(t; t_0) + o(\varepsilon^2). \quad (109)$$

Then, substituting Eq. (109) into Eq. (108) and equating the terms with the same powers of  $\varepsilon$ , we obtain

$$O(\varepsilon^0) : \frac{d^2 x_0}{dt^2} + x_0 = 0, \quad (110)$$

$$O(\varepsilon^1) : \frac{d^2 x_1}{dt^2} + x_1 = (1 - x_0^2) \frac{dx_0}{dt}, \quad (111)$$

$$O(\varepsilon^2) : \frac{d^2 x_2}{dt^2} + x_2 = (1 - x_0^2) \frac{dx_1}{dt} - 2x_0 x_1 \frac{dx_0}{dt}. \quad (112)$$

The solution for the zeroth-order equation (110) is

$$x_0(t; t_0) = A(t_0) \cos(t + \theta(t_0)), \quad (113)$$

where  $A$  and  $\theta$  are integral constants and they potentially depend on initial time  $t_0$ . Then, substituting Eq. (113) into Eq. (111), we have

$$\frac{d^2 x_1}{dt^2} + x_1 = -A \left( 1 - \frac{A^2}{4} \right) \sin(t + \theta) + \frac{A^3}{4} \sin(3t + 3\theta). \quad (114)$$

By solving the solution of Eq. (114) around  $t = t_0$ , the first-order solution is given by

$$x_1(t; t_0) = \frac{A}{2} \left( 1 - \frac{A^2}{4} \right) (t - t_0) \cos(t + \theta) - \frac{A^3}{32} \sin(3t + 3\theta). \quad (115)$$

Similarly, by substituting zero-th and first-order solutions (113) and (115) into Eq. (112), the second-order equation is

$$\begin{aligned} \frac{d^2 x_2}{dt^2} + x_2 = & F_1(A) \cos(t + \theta) - F_2(A)(t - t_0) \sin(t + \theta) + F_3(A) \cos(3t + 3\theta) \\ & - F_4(A)(t - t_0) \sin(3t + 3\theta) + F_5(A) \cos(5t + 5\theta), \end{aligned} \quad (116)$$

where

$$F_1(A) = \frac{A}{2} \left( \frac{13}{64}A^4 - A^2 + 1 \right), \quad (117)$$

$$F_2(A) = \frac{A}{2} \left( \frac{3}{16}A^4 - A^2 + 1 \right), \quad (118)$$

$$F_3(A) = \frac{A^3}{32} \left( \frac{5}{2}A^2 - 7 \right), \quad (119)$$

$$F_4(A) = \frac{3A^3}{8} \left( \frac{1}{4}A^2 - 1 \right), \quad (120)$$

$$F_5(A) = \frac{5A^5}{128}. \quad (121)$$

The solution of the second-order equation (116) is

$$\begin{aligned} x_2(t; t_0) = & \frac{1}{4}(2F_1(A) - F_2(A))(t - t_0) \sin(t + \theta) + \frac{1}{4}F_2(A)(t - t_0)^2 \cos(t + \theta) \\ & + \frac{1}{32}(-4F_3(A) + 3F_4(A)) \cos(3t + 3\theta) + \frac{1}{8}F_4(A)(t - t_0) \sin(3t + 3\theta) \\ & - \frac{1}{24}F_5(A) \cos(5t + 5\theta). \end{aligned} \quad (122)$$

Therefore, the perturbative solution up to the second-order of  $\varepsilon$  is

$$\begin{aligned} x(t; t_0) = & A \cos(t + \theta) + \varepsilon \left\{ \frac{A}{2} \left( 1 - \frac{A^2}{4} \right) (t - t_0) \cos(t + \theta) - \frac{A^3}{32} \sin(3t + 3\theta) \right\} \\ & + \varepsilon^2 \left\{ \frac{1}{4}(2F_1(A) - F_2(A))(t - t_0) \sin(t + \theta) + \frac{1}{4}F_2(A)(t - t_0)^2 \cos(t + \theta) \right. \\ & + \frac{1}{32}(-4F_3(A) + 3F_4(A)) \cos(3t + 3\theta) + \frac{1}{8}F_4(A)(t - t_0) \sin(3t + 3\theta) \\ & \left. - \frac{1}{24}F_5(A) \cos(5t + 5\theta) \right\} + o(\varepsilon^2). \end{aligned} \quad (123)$$

To obtain the globally valid solution using Eq. (123), we apply the RG method, which utilizes the RG equation

$$\begin{aligned} \frac{dx}{dt_0} \Big|_{t_0=t} = & \left\{ \frac{dA}{dt} + \varepsilon \frac{1}{2}A \left( \frac{1}{4}A^2 - 1 \right) \right\} \cos(t + \theta) \\ & + \left\{ -A \frac{d\theta}{dt} - \varepsilon^2 \frac{1}{4}(2F_1(A) - F_2(A)) \right\} \sin(t + \theta) = 0, \end{aligned} \quad (124)$$

where we have neglected the higher-order terms  $o(\varepsilon^2)$ . For Eq. (124) to hold for any  $t$ , the coefficients of the two independent functions should vanish. Thus, we end up with the dynamical

equations for  $A$  and  $\theta$

$$\frac{dA}{dt} = \frac{1}{2}\varepsilon A \left(1 - \frac{1}{4}A^2\right) \quad (125)$$

$$\frac{d\theta}{dt} = -\varepsilon^2 \frac{1}{4A} (2F_1(A) - F_2(A)) = -\varepsilon^2 \frac{1}{8} \left(\frac{7}{32}A^4 - A^2 + 1\right) \quad (126)$$

Equation (125) has two fixed points, namely  $A = 0$  and  $2$ . The amplitude  $A$  asymptotically approaches  $A = 2$ , which is the limit cycle. Therefore, the dynamical behavior of  $\theta(t)$  on the limit cycle reads

$$\theta(t) = -\varepsilon^2 \frac{1}{16}t + \theta_0, \quad (127)$$

where  $\theta_0$  is the initial phase at  $t = 0$ . Thus, the globally valid solution on the limit cycle is given by

$$x(t) = 2 \cos(\omega t + \theta_0) - \varepsilon \frac{1}{4} \sin(3\omega t + 3\theta_0) - \varepsilon^2 \frac{3}{32} \cos(3\omega t + 3\theta_0) - \varepsilon^2 \frac{5}{96} \cos(5\omega t + 5\theta_0) + o(\varepsilon^2), \quad (128)$$

where the angular frequency  $\omega$  up to the second order is expressed as

$$\omega = 1 - \varepsilon^2 \frac{1}{16} + o(\varepsilon^2). \quad (129)$$

Using Eqs. (128) and (129), the period and  $NS$  of the van der Pol model read

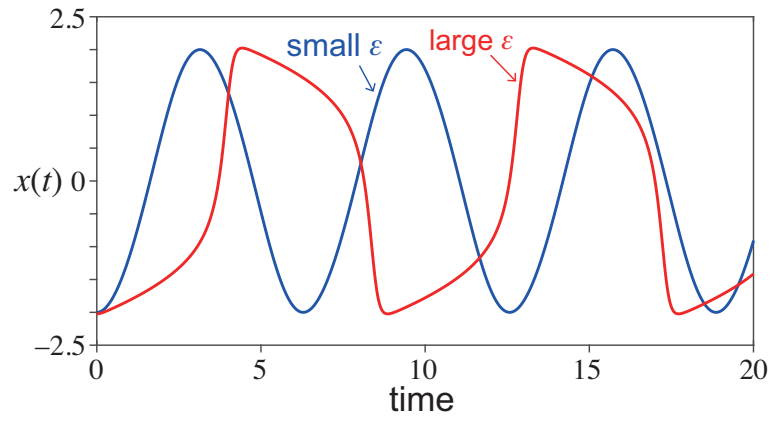
$$\tau = \frac{2\pi}{\omega} = \frac{2\pi}{1 - \varepsilon^2/16 + o(\varepsilon^2)} = 2\pi \left(1 + \varepsilon^2 \frac{1}{16} + o(\varepsilon^2)\right), \quad (130)$$

$$NS = \left[ \frac{\sum_{j=1}^{\infty} |a_j|^2 j^2}{\sum_{j=1}^{\infty} |a_j|^2} \right]^{\frac{1}{2}} = \left[ \frac{1 + \varepsilon^2(9/64) + o(\varepsilon^2)}{1 + \varepsilon^2/64 + o(\varepsilon^2)} \right]^{\frac{1}{2}} = 1 + \varepsilon^2 \frac{1}{16} + o(\varepsilon^2), \quad (131)$$

Accordingly,

$$\tau = 2\pi NS. \quad (132)$$

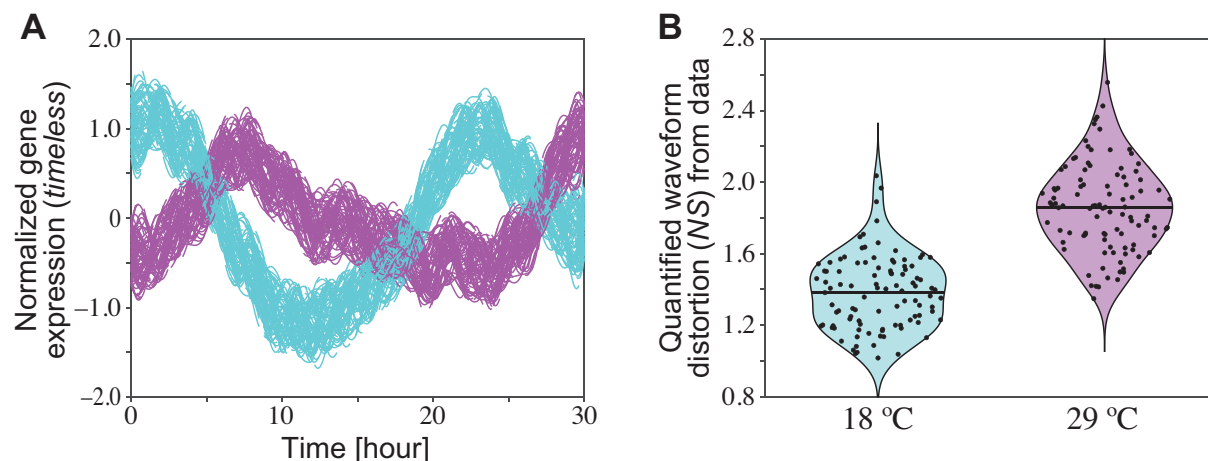
This expression clearly illustrates that the period  $\tau$  and the waveform distortion  $NS$  in the van



Supplementary Figure 2: The waveform examples of the van der Pol model. The parameter value is  $\varepsilon = 0.1$  (blue) and  $\varepsilon = 3$  (red).

der Pol model tend to increase (or decrease) together in a proportional manner, which was also demonstrated using signal processing methods (Supplementary Fig. 2) [31].

## Supplementary Figures



Supplementary Figure 3: Analysis of the circadian waveform of the *Drosophila* mutant *perL* at different temperatures using previously reported experimental data [55]. (A) Re-plot of Fig. 4B in [55]. The average curves of *tim-luc* at 18 and 29°C are extracted using WebPlotDigitizer at 1-h intervals. Noise uniformly distributed between  $-0.4$  and  $0.4$  is added to generate 100 time series datasets. Spline interpolation is applied to set the sampling interval to 0.1 h. The interpolated time series data at 18 (cyan) and 29 °C (magenta) are plotted. (B) Distribution of the quantified waveform distortion ( $NS$ ) from the data at 18 (cyan) and 29 °C (magenta). The noisy time series data are detrended by multiplying an exponential function to align local maxima at 18 °C or local minima at 29 °C. The Fourier coefficients of the detrended time-series are quantified using GHA.  $NS$  values were estimated from the coefficients up to the third harmonics. Dots represent the  $NS$  values for each data set, and horizontal lines represent their average values.



## Supplementary Tables

Supplementary Table 1: Activation energies and frequency factors for each reaction in Fig. 1

Parameter	Activation Energy, $E_i$	Frequency Factor, $A_i$
$k_1$	$1.39 \times 10^4$	40.0
$k_2$	$6.31 \times 10^3$	2.31
$k_3$	$2.89 \times 10^3$	0.515
$p_1$	$1.94 \times 10^4$	229
$p_2$	$7.03 \times 10^3$	2.44
$r$	$8.11 \times 10^4$	$1.06 \times 10^{13}$

Supplementary Table 2: Parameter values for each reaction in Fig. 3B-C and Fig. 6.

Parameter	Fig. 3B and Fig. 6		Fig. 3C	
	slow	fast	slow	fast
$k_1$	0.269	0.296	0.247	0.278
$k_2$	0.200	0.221	0.192	0.213
$k_3$	0.0817	0.150	0.0662	0.112
$p_1$	0.290	0.328	0.160	0.219
$p_2$	0.246	0.376	0.256	0.312
$r$	0.180	0.226	0.244	0.314
$n$	15	15	13	13